A national laboratory of the U.S. Department of Energy
Office of Energy Efficiency & Renewable Energy

National Renewable Energy Laboratory

Innovation for Our Energy Future

High-Efficiency Amorphous Silicon and Nanocrystalline Silicon-Based Solar Cells and Modules

Annual Technical Progress Report
30 January 2006 – 29 January 2007

S. Guha and J. Yang
United Solar Ovonic LLC
Troy, Michigan

Subcontract Report
NREL/SR-520-41866
July 2007

NREL is operated by Midwest Research Institute • Battelle Contract No. DE-AC36-99-GO10337

High-Efficiency Amorphous Silicon and Nanocrystalline Silicon-Based Solar Cells and Modules

Annual Technical Progress Report 30 January 2006 – 29 January 2007

S. Guha and J. Yang
United Solar Ovonic LLC
Troy, Michigan

NREL Technical Monitor: Bolko von Roedern

Prepared under Subcontract No. ZXL-6-44205-14

Subcontract Report
NREL/SR-520-41866
July 2007

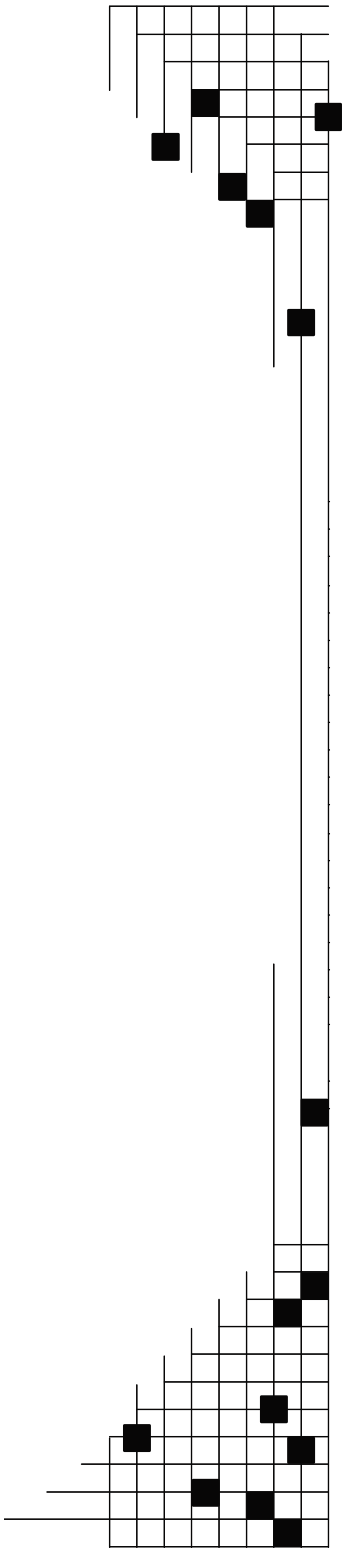

National Renewable Energy Laboratory
1617 Cole Boulevard, Golden, Colorado 80401-3393
303-275-3000 • www.nrel.gov

Operated for the U.S. Department of Energy
Office of Energy Efficiency and Renewable Energy
by Midwest Research Institute • Battelle

Contract No. DE-AC36-99-GO10337

Table of Contents

List of Figures

List of Tables

Preface

This annual report covers the work performed by United Solar Ovonic LLC for the period from January 30, 2006 to January 29, 2007, under the support of the Thin Film Partnership Subcontract No. ZXL-6-44205-14. The following personnel participated in this research program.

A. Banerjee, E. Chen, G. Ganguly, S. Guha (Principal Investigator), B. Hang, M. Hopson, A. Mohsin, J. Noch, J. M. Owens, T. Palmer, L. Sivec, D. Wolf, B. Yan, J. Yang (Co-Principal Investigator), K. Younan, G. Yue, and X. Xu.

Collaboration with the Colorado School of Mines, University of Oregon, Syracuse University, and the National Renewable Energy Laboratory is acknowledged. We would like to thank S. R. Ovshinsky and H. Fritzsche for their constant encouragement and useful discussion.

Executive Summary

Objectives

United Solar Ovonic LLC (United Solar) has successfully used its spectrum splitting a-Si:H/a-SiGe:H/a-SiGe:H triple-junction structure in the two ~30 MW manufacturing plants, and will use the same technology in its next 60 MW plant in Greenville Michigan, which will start production in 2007. In order to improve the solar panel efficiency and reduce the manufacturing cost further, we have identified three areas of research for this project:

i) Optimize the a-Si:H and a-SiGe:H deposition parameters under the current manufacturing constraints for improving the solar module efficiency and manufacturing throughput, and reducing the manufacturing cost.

ii) Explore new deposition methods for a-Si:H and a-SiGe:H materials to improve the a-Si:H/a-SiGe:H/a-SiGe:H triple-junction cell efficiency at high deposition rate.

iii) Explore new materials and new cell structures for higher efficiency at high deposition rate.

The first area represents a short-term goal with the objective of improving the current manufacturing module efficiency and throughput without modification of the production line. Therefore, certain constraints have to be considered. For example, the deposition rate of each layer has to be adjusted according to the web speed and chamber length. Under this premise, any improvement in the cell efficiency will improve the current manufacturing module efficiency and throughput. The second area represents an intermediate-term goal with the objective of considerably improving cell and module efficiency with a higher throughput but with limited modifications of the manufacturing machines. The third area represents a long-term goal with the objective of significantly improving the module efficiency with high throughput by using new designs for the manufacturing machines in order to deposit the new materials.

Approaches

For the first area, we have carried out research with a two-step approach. We first optimized the a-Si:H and a-SiGe:H component cells as well as the a-Si:H/a-SiGe:H/a-SiGe:H triple-junction cells using one of our large-area batch RF glow discharge machines. The a-Si:H/a-SiGe:H/a-SiGe:H triple-junction cells are deposited on Al/ZnO back reflector made in the manufacturing machines. When experimental deposition parameters are improved, the new recipe will be transferred to the production line.

For the second area, we have studied high rate a-Si:H and a-SiGe:H solar cells made with MVHF for a few years. We have continued on this track for high rate deposition. Although the MVHF a-Si:H top cell has shown a significant advantage over the RF deposited a-Si:H cells at high rates, many challenges still exist, especially in the quality of high rate a-SiGe:H middle and bottom cells. In this project, we explored more deposition parameters and researched new deposition regimes.

In the last ten years, nc-Si:H has attracted significant attention as a potential substitute for a-SiGe:H in multi-junction solar cells due to the improved stability and long wavelength response. United Solar has studied nc-Si:H materials and solar cells for several years. For the third area, we continued investigating issues related to nc-Si:H material properties, cell efficiency, and deposition rate. The major target is to demonstrate the feasibility of using nc-

Si:H in multi-junction structures and to achieve higher cell and module efficiencies than those achieved using the conventional a-Si:H/a-SiGe:H/a-SiGe:H triple-junction structure. We have identified that the nanocrystalline evolution along the growth direction is one of the major challenges for high efficiency nc-Si:H solar cells. Therefore, we developed a hydrogen dilution profiling technique for controlling the nanocrystalline evolution during nc-Si:H deposition. We have further optimized hydrogen dilution for high rate nc-Si:H deposition. At the same time, we improved the structure of the MVHF deposition chamber to make it suitable for high-pressure deposition. In addition, we optimized the a-Si:H top cell and a-SiGe:H middle cell for high efficiency a-Si:H/a-SiGe:H/nc-Si:H triple-junction structure.

Another major issue in using nc-Si:H solar cells in a production line is the thickness of the absorbed layer and its uniformity. Due to the decrease of electromagnetic wavelength with the increase of VHF frequency, the electric field distribution over large-area cathode becomes non-uniform. A special design for the large-area VHF cathodes is required to achieve uniform deposition. We have worked on the large-area VHF cathode design for the nc-Si:H deposition.

Through collaboration with NREL, University of Oregon, Colorado School of Mines, and Syracuse University, we also investigated the a-Si:H, a-SiGe:H, and nc-Si:H material properties and mechanism of light-induced degradation in these materials and solar cells. Most results have been reported by our collaborators.

Status/Accomplishments

1. We have achieved an aperture-area stable efficiency of 8.6% on an a-Si:H/a-SiGe:H/a-SiGe:H triple-junction solar cell deposited under the manufacturing constraints on an Al/ZnO back reflector made in the manufacturing line. The cell was encapsulated using a procedure similar to the manufacturing process.
2. We have investigated deposition parameters for a-Si:H and a-SiGe:H deposition with MVHF at high rates. We found that the performance and stability of a-Si:H single-junction cells deposited with MVHF do not depend on the deposition rate in the range of 1-15 Å/s.
3. We have achieved active-area (0.25 cm^2) initial and stable efficiencies of 9.0% and 8.5%, respectively, for nc-Si:H single-junction cells made with MVHF at a high rate ~ 5-8 Å/s.
4. We have achieved active-area (0.25 cm^2) initial and stable efficiencies of 15.1% and 13.0%, respectively, for an a-Si:H/a-SiGe:H/nc-Si:H triple-junction cell, where the top and middle cells were made using RF at a low rate ~ 1 Å/s, and the nc-Si:H bottom cell using MVHF at a high rate ~ 5-8 Å/s.
5. We have achieved active-area (0.25 cm^2) initial and stable efficiencies of 14.1% and 13.3%, respectively, for an a-Si:H/nc-Si:H/nc-Si:H triple-junction cell, where the top cell was made using RF at a low rate ~ 1 Å/s, and the nc-Si:H middle and bottom cells using MVHF at a high rate ~ 5-8 Å/s.
6. We have demonstrated that an optimized hydrogen dilution profiling not only improves the initial nc-Si:H cell performance but also the stability against light soaking.

Publications

1. G. Yue, B. Yan, G. Ganguly, J. Yang, S. Guha, and C. Teplin, "Material Structure and Metastability of Hydrogenated Nanocrystalline Silicon Solar Cells," Appl. Phys. Lett. **88**, 263507 (2006).
2. G. Yue, B. Yan, G. Ganguly, J. Yang, and S. Guha, "Metastability of Hydrogenated Nanocrystalline Silicon Solar Cells," Mater. Res. Soc. Symp. Proc. **910**, A02-01 (2006). (Invited).
3. B. Yan, J. Yang, and S. Guha, "Temperature Dependence of Dark Current-Voltage Characteristics of Hydrogenated Amorphous and Nanocrystalline Silicon Based Solar Cells," Mater. Res. Soc. Symp. Proc. **910**, A26-02 (2006).
4. B. Yan, C.-S. Jiang, H. R. Moutinho, M. M. Al-Jassim, J. Yang, and S. Guha, "Local Current Flow in Mixed-Phase Silicon Solar Cells and Correlation to Light-Induced Open-Circuit Voltage Enhancement," Mater. Res. Soc. Symp. Proc. **910**, A23-06 (2006).
5. P. G. Hugger, S. Datta, P.T. Erslev, G. Yue, G. Ganguly, B. Yan, J. Yang, S. Guha, and J.D. Cohen, **"**Electronic Characterization and Light-Induced Degradation in nc-Si:H Solar Cells," Mater. Res. Soc. Symp. Proc. **910**, A01-05 (2006).
6. D. C. Bobela, T. Su, P. C. Taylor, A. Madan, and G. Ganguly, "The Concentration of $(SiH_2)n$ Sites in Low and High Defect Density a-Si:H," Mater. Res. Soc. Symp. Proc. **910**, A09-04 (2006).
7. N. H. Nickel, M. Weizman, I. Sieber, and B. Yan, "Influence of Compositional and Structural Changes on Hydrogen Bonding in Silicon and Silicon-Germanium Alloys," J. of Non-Crystalline Solids **352**, 1037 (2006).
8. D. C. Bobela, T. Su, P. C. Taylor, and G. Ganguly, "Microscopic Properties of Silicon Dihydride Bonding in a-Si:H," J. of Non-Crystalline Solids **352**, 1041 (2006).
9. M. Weizman, N. H. Nickel, I. Sieber, and B. Yan, "Successive Segregation in Laser-Crystallized Poly-SiGe Thin Films," J. of Non-Crystalline Solids **352**, 1259 (2006).
10. S. Guha and J. Yang, "Progress in Amorphous and Nanocrystalline Silicon Solar Cells," J. of Non-Crystalline Solids **352**, 1917 (2006).
11. B. Yan, G. Yue, J.M. Owens, J. Yang, and S. Guha, "Over 15% Efficient Hydrogenated Amorphous Silicon Based Triple-Junction Solar Cells Incorporating Nanocrystalline Silicon", Conf. Record of the 2006 IEEE 4th World Conf. on Photovoltaic Energy Conversion, (Hawaii, USA, May 7-12, 2006), p. 1477.
12. C.-S. Jiang, H. R. Moutinho, M. M. Al-Jassim, L. L. Kazmerski, B. Yan, J. M. Owens, J. Yang, and S. Guha, "Distribution of Local Open-Circuit Voltage on Amorphous and Nanocrystalline Mixed-Phase Si:H and SiGe:H Solar Cells," Conf. Record of the 2006 IEEE 4th World Conf. on Photovoltaic Energy Conversion, (Hawaii, USA, May 7-12, 2006), p. 1552.
13. G. Yue, B. Yan, G. Ganguly, J. Yang, S. Guha, C. Teplin, and D. L. Williamson, "Performance Improvement of Hydrogenated Nanocrystalline Silicon Solar Cells by Hydrogen Dilution Profiling," Conf. Record of the 2006 IEEE 4th World Conf. on Photovoltaic Energy Conversion, (Hawaii, USA, May 7-12, 2006), p. 1588.
14. G. Ganguly, G. Yue, B. Yan, J. Yang, and S. Guha, "Fabrication of Large Area Amorphous Silicon/Nanocrystalline Silicon Double Junction Solar Cells," Conf. Record of the 2006 IEEE 4th World Conf. on Photovoltaic Energy Conversion, (Hawaii, USA, May 7-12, 2006), p. 1712.
15. B. Yan, C.-S. Jiang, C. W. Teplin, H. R. Moutinho, M. M. Al-Jassim, J. Yang, and S. Guha "Local Current Flow in Amorphous and Nanocrystalline Mixed-Phase Silicon Solar Cells", J. Appl. Phys. **101**, 033711 (2007).

1. Large-Area a-Si:H/a-SiGe:H/a-SiGe:H Triple-Junction Cells Made Under the Manufacturing Constraints

1.1. Introduction

One of our major objectives for this project is to develop new deposition parameters for improving solar cell efficiency and throughput, and hence reducing the cost of manufacturing. The spectrum splitting a-Si:H/a-SiGe:H/a-SiGe:H triple-junction structure on Al/ZnO back reflector is used in our two ~30 MW manufacturing lines and will be used in the next 60 MW manufacturing plant in Greenville, Michigan. Therefore, one task of the project is to optimize the deposition parameters of a-Si:H/a-SiGe:H/a-SiGe:H triple-junction solar cells under the manufacturing constraints, mainly the deposition time of each layer. Previously, we have achieved a stable total-area (0.268 cm^2) cell efficiency of 9.1% and stable aperture-area (460 cm^2) module efficiency of 8.9% using our large-area batch machine. Those cells were deposited with Si_2H_6 and GeH_4 mixtures under the manufacturing constraints on Al/ZnO back reflectors. In order to reduce cost, we have switched to SiH_4 and GeH_4 mixtures in the manufacturing process. In the research and development department, we have also studied the optimization of the deposition conditions using the SiH_4 and GeH_4 mixtures. We achieved a stable total-area (0.268 cm^2) triple-junction cell efficiency of 9.1%, which is similar to the result obtained with the Si_2H_6 and GeH_4 mixture. This result showed that, in principle, one can achieve a similar performance using inexpensive SiH_4 instead of Si_2H_6. In Phase I of this project, we have carried out optimization of large-area deposition of a-Si:H/a-SiGe:H/a-SiGe:H triple-junction solar cells using SiH_4 and GeH_4 gas mixtures. Al/ZnO back reflectors made in the product machines were used.

1.2. Experimental Details

We used one of our large-area (14×15 in^2) batch machines (2B) for the deposition of a-Si:H and a-SiGe:H intrinsic layers as well as the doped layers. The deposition time of each layer is fixed according to the calculation with the web speed and the chamber lengths of the production line. The optimization of cell performance and uniformity were carried out using small Indium Tin Oxide (ITO) dots with an active-area of 0.25 cm^2. Large-area (>400 cm^2) modules were made using the center area of the substrate with wires and bus bars. The large-area modules were encapsulated with a procedure similar to that used in the manufacturing process. The small-area cells were measured using an AM1.5 ORC solar simulator with quantum efficiency (QE) correction for the short-circuit current density. The large-area modules were measured at various states of light soaking using a Spire solar simulator with an NREL calibrated c-Si solar cell with a proper filter. The light soaking experiments were done under 100 mW/cm^2 white light at 50 °C for over 1000 hours.

1.3. Small Area Cell Performance and Uniformity

The uniformity of thickness and cell performance is a major concern for large-area deposition. In order to obtain high module efficiency, the cell performance has to satisfy certain uniformity requirements. We deposited the samples on a large-area (14×15 in^2) substrate and then cut them into 1.85×1.85 in^2 pieces at different locations. Since we normally make 8.5×8.5 in^2 modules, we cut nine pieces from an area 9.2×9.2 in^2. One is in the center of the substrate,

one at the middle of each of the four edges, and one at each of the four corners of the 9.2×9.2 in^2 area. Sixteen small ITO dots, with an active area of 0.25 cm^2, were deposited on the nine pieces for J-V and QE measurements. Table I lists the cell performance from one run (2B 11147). The J-V data for each location are averages of the measurements on four cells. The uniformity of the cell performance in the given area is reasonably good. The highest initial J-V measured active-area efficiency is 11.06% (QE corrected 10.92%), and the average is 10.62% with a non-uniformity of ±5%. This uniformity is acceptable for large-area modules.

1.4. Large Area Module

Several large-area modules have been made with the same deposition recipe as the cells shown in Table I (2B 11147). The modules were measured at the states before and after lamination, as well as light soaked states for different times. Table II lists the aperture-area performance of four modules. The data presented here are as-measured data without spectral mismatch corrections. The encapsulation causes a decrease of 1-4% in J_{sc}, 0.4-1.0% in V_{oc}, but an increase of 0-1.5% in FF. The major light-induced degradation appears in the first 500 hours. The change in the last 500 hours is very small. The average light-induced degradation is about 15.7%, which is similar to that observed in our previous experiments of a-Si:H/a-SiGe:H/a-SiGe:H triple-junction solar cells. The major change is in the FF, where an average of 10.6% reduction appears after light soaking. The best stable aperture-area efficiency is 8.6%, which is slightly lower than the best module efficiency of 8.9% achieved using a Si_2H_6 and GeH_4 mixture. Figure 1 shows the I-V characteristics of the best module in the three states.

It is well known that the efficiency measured under a given solar simulator with a calibrated reference cell is not necessarily the same as under the standard AM1.5 illumination due to the difference in their spectra. Normally two major errors appear in J_{sc} and FF. First is the difference between the spectrum of the light source and the ideal AM1.5 spectrum as well as the difference in the QE spectra of the testing and reference cells, both of which cause an error in J_{sc}. Second, the non-ideal AM1.5 spectrum of the light source causes a difference in the current mismatching of the component cells, which results in an error in FF.

Table I. J-V characteristics of a-Si:H/a-SiGe:H/a-SiGe:H triple-junction cells at different locations of a large-area cell , where the J_{sc} was taken directly from the J-V measurements. QE current densities and QE corrected efficiency (Eff^Q) of five cells are listed as a reference.

Location in 2B 11147	J_{sc} (mA/cm^2)	V_{oc} (V)	FF	Eff (%)	Eff^Q (%)	QE (mA/cm^2)		
						Top	Mid.	Bot.
Left North	7.41	2.195	0.656	10.67				
Left Center	7.40	2.220	0.659	10.82				
Left South	7.27	2.238	0.663	10.78	10.62	7.28	7.16	7.36
Central North	7.18	2.238	0.688	11.06	10.92	7.09	7.20	7.22
Central Center	7.24	2.237	0.679	10.98	10.66	7.02	7.31	7.28
Central South	7.22	2.207	0.676	10.77	10.49	7.03	7.49	7.32
Right North	7.47	2.161	0.623	10.05				
Right Center	7.49	2.122	0.634	10.28	9.83	7.31	7.41	7.48
Right South	7.38	2.159	0.636	10.14				
Average	7.34	2.197	0.657	10.62				

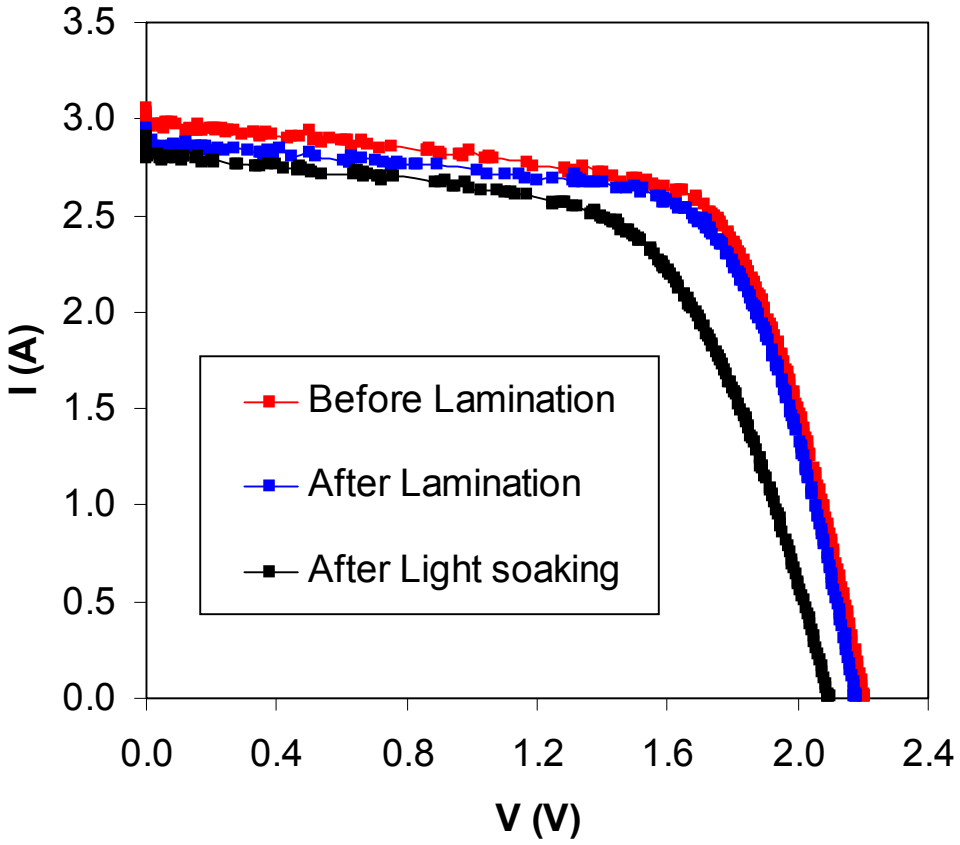

Figure 1. I-V characteristics of an a-Si:H/a-SiGe:H/a-SiGe:H triple-junction solar cell (2B 10383) before and after lamination, as well as after light soaking.

In principle, the error in the J_{sc} of a single-junction solar cell can be corrected by adjusting the light intensity of the solar simulator based on a spectrum mismatching (M) factor [1]. The calculation of the M factor involves the reference light source (AM1.5) spectrum, the test light source (solar simulator) spectrum, the QE curve of reference cell and the QE curve of the test cell. In order to obtain a corrected J_{sc}, one can change the test light intensity by a factor of 1/M or use the measured J_{sc} under the standard setting condition and divide it by the M factor.

Theoretically, the M-factor correction can provide a more accurate measurement of J_{sc}. However, in practice, more errors could be introduced by the errors in the QE of the testing cell. The major problem is that it is hard to measure the QE of large-area modules. An alternative way is to use the QE measured from a different cell with a small area but made under the same condition. In most cases, one uses QE data from a small-area cell without encapsulation. It is well known that the encapsulation changes the QE curves and therefore, the M factor.

Table II. Summary of a-Si:H/a-SiGe:H/a-SiGe:H triple-junction module performance in different states. Eff^T(%) is temperature corrected efficiency at 25 °C.

Sample 2B#	State	Area (cm^2)	T (^oC)	I_{sc} (A)	J_{sc} (mA/cm^2)	V_{oc} (V)	FF	P_{max} (W)	Eff (%)	Eff^T(%)
10386	Before lamination	420.0	24.2	2.960	7.05	2.190	0.654	4.24	10.09	10.08
	After lamination	413.8	24.2	2.882	6.96	2.180	0.662	4.16	10.05	10.04
	Change due to lamination				-1.3%	-0.5%	1.2%			-0.4%
	585-hour light soaking	413.8	24.2	2.820	6.81	2.100	0.606	3.58	8.65	8.64
	1004-hour light soaking	413.8	25.1	2.813	6.80	2.090	0.599	3.52	8.51	8.51
	Change due to light soaking				-2.3%	-4.1%	-9.5%			-15.2%
10383	Before lamination	420.0	23.9	2.947	7.02	2.210	0.662	4.31	10.25	10.24
	After lamination	416.0	25.1	2.876	6.91	2.180	0.671	4.20	10.10	10.11
	Change due to lamination				-1.6%	-1.4%	1.3%			-1.3%
	585-hour light soaking	416.0	24.4	2.833	6.81	2.100	0.616	3.66	8.80	8.80
	1004-hour light soaking	416.0	24.9	2.811	6.76	2.100	0.609	3.59	8.63	8.63
	Change due to light soaking				-2.2%	-3.7%	-9.2%			-14.6%
11156	Before lamination	462.0	23.7	3.382	7.32	2.230	0.645	4.87	10.54	10.53
	After lamination	458.0	24.2	3.239	7.07	2.220	0.654	4.70	10.26	10.25
	Change due to lamination				-3.4%	-0.4%	1.4%	-3.5%	-2.6%	-2.7%
	585-hour light soaking	458.0	24.7	3.236	7.07	2.13	0.584	4.02	8.78	8.78
	1004-hour light soaking	458.0	24.9	3.231	7.05	2.12	0.569	3.89	8.50	8.50
	Change due to light soaking				-0.3%	-4.5%	-13.1%			-17.0%
11166	Before lamination	462.0	23.7	3.349	7.25	2.230	0.650	4.85	10.50	10.47
	After lamination	458.0	24.4	3.215	7.02	2.210	0.651	4.63	10.11	10.10
	Change due to lamination				-3.2%	-0.9%	0.2%	-4.5%	-3.7%	-3.5%
	585-hour light soaking	458.0	24.4	3.199	6.98	2.110	0.581	3.92	8.56	8.55
	1004-hour light soaking	458.0	25.4	3.176	6.93	2.110	0.578	3.88	8.47	8.47
	Change due to light soaking				-1.3%	-4.5%	-11.2%			-16.1%

In this study, we tried to make the measurement more accurate by using QE data that are close to the QE of real modules. We used adjacent pieces from the module fabrication and made small-area (1.2 cm^2) cells with the same wires and bus bars as used in the module fabrication. We also encapsulated the small-area cells and light soaked them using the same procedures as the large-area modules. The QE curves were measured at different states for calculating the M factor. Table III lists the J-V characteristics and QE current densities of four small-area cells from two large-area depositions that were used for module fabrication. It appears that the small-area cells have a slightly smaller V_{oc} and J_{sc}, but a slightly larger FF than the large-area modules at each corresponding state, which could be due to the non-uniformity of the deposition. Figure 2 gives an example of the QE changes from the initial non-encapsulated state to the encapsulated and light-soaked states. Corresponding reflection curves are also presented. The QE curves change dramatically at the short wavelength below 400 nm. We calculated the M-factors of the four cells at the initial non-encapsulated state and the encapsulated and light soaked state using the measured QE data and the QE of our reference cell as well as the spectrum of our Spire solar simulator. Table IV summarizes the M-factors of four cells at the three states. On average, the M factor is about 0.965 in the initial non-encapsulated state, and 0.983 in the final encapsulated and light-soaked state. If we take the M factor into account, the highest stable encapsulated module efficiency should be 8.78%.

1.5. Summary

We have optimized large-area deposition of a-Si:H/a-SiGe:H/a-SiGe:H triple-junction solar cells under the manufacturing constraints and SiH_4 and GeH_4 gas mixture on Al/ZnO back reflectors from the manufacturing line. A stable aperture-area (416 cm^2) efficiency of 8.6% has been achieved. With the spectrum mismatching correction, this efficiency could be 8.8%, which is similar to the highest module efficiency previously achieved using a Si_2H_6 and GeH_4 gas mixture.

Table III. Summary of J-V characteristics of a-Si:H/a-SiGe:H/a-SiGe:H triple-junction solar cells at various states. The small area (1.2 cm^2) samples were taken from adjacent sections of the large area modules 2B 11156 and 11166 shown in Table II. B-Lam represents the state before lamination; L-Soak represents the state after lamination and light soaking.

Sample #	State	Eff (%)	J_{sc} (mA/cm^2)	V_{oc} (V)	FF	QE (mA/cm^2)		
						Top	Middle	Bottom
11156-3	B-Lam	9.85	6.77	2.168	0.671	6.77	7.30	7.01
	L-Soak	8.20	6.60	2.079	0.598	6.60	7.26	6.88
11156-5	B-Lam	10.12	6.97	2.177	0.667	6.97	7.39	7.23
	L-Soak	8.18	6.64	2.074	0.594	6.64	7.20	7.08
11166-1	B-Lam	10.34	6.90	2.226	0.673	7.01	6.90	6.99
	L-Soak	8.40	6.67	2.125	0.593	6.73	6.67	6.78
11166-3	B-Lam	10.34	6.93	2.230	0.669	6.97	6.93	7.07
	L-Soak	8.38	6.61	2.124	0.597	6.61	6.72	6.85

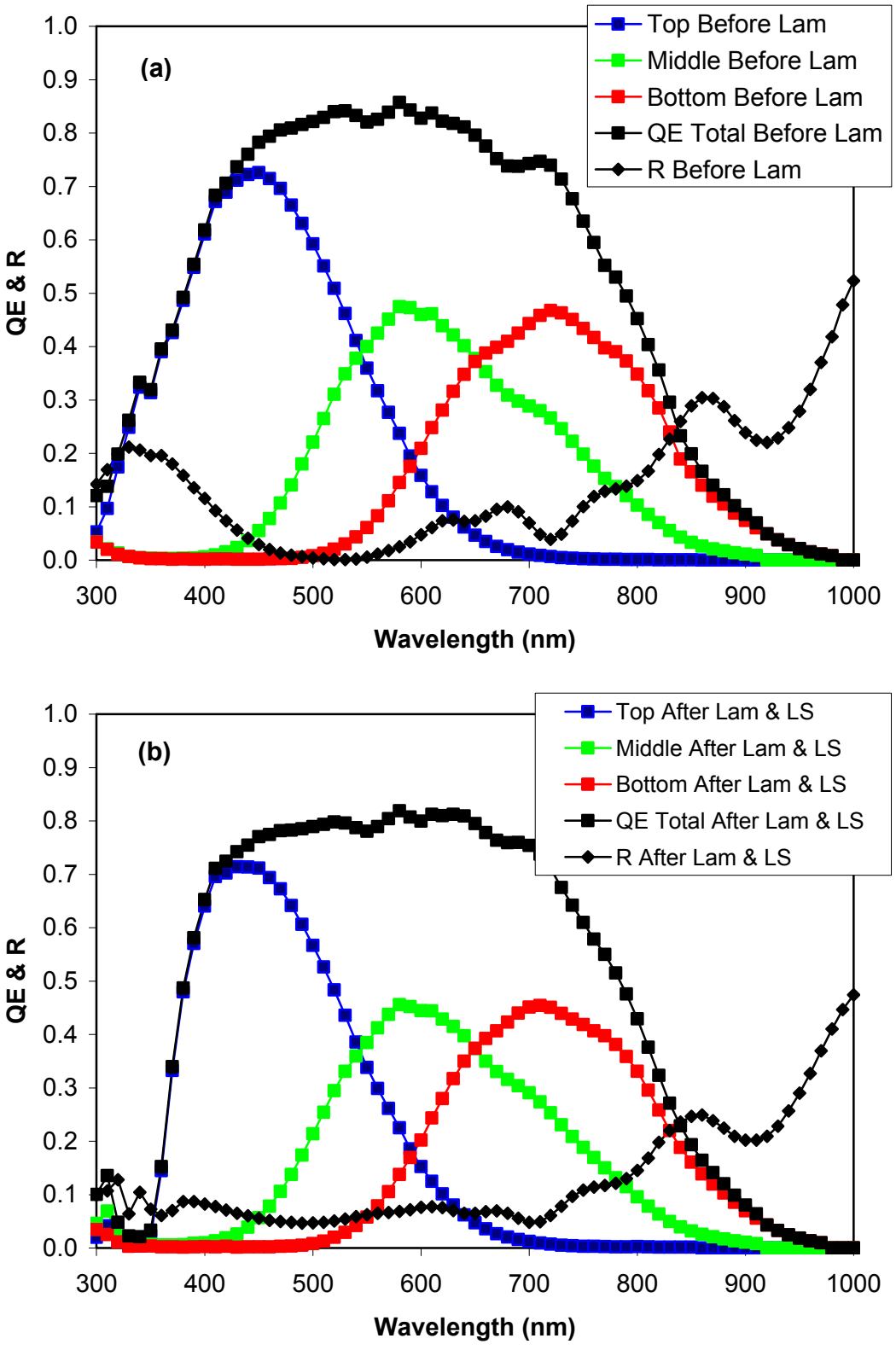

Figure 2. Quantum efficiency (QE) and reflection (R) curves of an a-Si:H/a-SiGe:H/a-SiGe:H triple-junction cell on Al/ZnO (a) before lamination and (b) after lamination and light soaking.

Table IV. The M factor of a-Si:H/a-SiGe:H/a-SiGe:H the small-area triple-junction solar cells in Table III in the states before and after lamination (Lam) as well as after light soaking (LS). The United Solar Spire solar simulator spectrum was used.

Sample #	State	M Factor			
		Top	Middle	Bottom	Overall
11156-3	Before Lam	0.957	1.024	1.060	0.957
	After Lam	0.981	1.024	1.060	0.981
	After LS	0.980	1.023	1.060	**0.980**
11156-5	Before Lam	0.959	1.024	1.066	0.959
	After Lam	0.981	1.024	1.062	0.981
	After LS	0.981	1.023	1.022	**0.981**
11166-1	Before Lam	0.961	1.023	1.065	0.967
	After Lam	0.981	1.026	1.064	0.981
	After LS	0.981	1.024	1.065	**0.991**
11166-3	Before Lam	0.977	1.024	1.064	0.977
	After Lam	0.981	1.025	1.065	0.981
	After LS	0.981	1.024	1.065	**0.981**

2. High Rate Deposition of a-Si:H and a-SiGe:H Solar Cells Using Modified Very High Frequency Glow Discharge

2.1. Introduction

A high deposition rate for making solar cell intrinsic layers is always desirable to increase throughput and reduce production cost. However, a-Si:H solar cells made with the conventional radio frequency (RF) glow discharge at high rates exhibit poor quality. The materials contain a high defect density, microvoids, and dihydride structures, which lead to a low initial efficiency and poor stability in solar cells. In order to reduce manufacturing costs, new deposition techniques are needed to increase the deposition rate without compromising the material quality. Obviously, increasing the deposition rate will directly increase the annual capacity or reduce the initial capital investment on the machine.

Very high frequency (VHF) glow discharge has been widely used in the deposition of a-Si:H [2] and nc-Si:H [3-5] materials and devices. Compared to the conventional RF technique, VHF plasma has higher electron density and lower ion energy, which is believed to increase the deposition rate and improve the material quality. In our laboratory, we have used a modified VHF (MVHF) system to make a-Si:H, a-SiGe:H [6-7], and nc-Si:H [8-9] solar cells. An initial efficiency of 11.2% was obtained in an a-Si:H/a-SiGe:H double-junction solar cell with the top cell intrinsic layer deposited at 8 Å/s and the bottom cell at 6 Å/s [7]. We have achieved an initial active-area efficiency of 9.0% on a nc-Si:H single-junction solar cell and a stabilized active efficiency of 13.3% on an a-Si:H/nc-Si:H/nc-Si:H triple junction solar cell [10]. In this study, we have optimized the deposition condition of a-Si:H in a wider growth parameter space, mainly in the higher pressure and smaller gap spacing regime. We have systematically studied the initial cell performance and stability as a function of the deposition rate.

2.2. a-Si:H Single-Junction Solar Cells Made With MVHF at High Deposition Rates

A series of a-Si:H *n-i-p* solar cells has been made using an MVHF high rate a-Si:H intrinsic layer and low rate RF doped layers. Under each deposition condition, two runs were made: one on a specular stainless steel (SS) substrate and one on a Ag/ZnO back reflector (BR) coated SS substrate. The deposition rate of the a-Si:H intrinsic layer was changed from 5 to 14 Å/s by varying the VHF power and the pressure. The thickness of the intrinsic layer was controlled in the range of 200-220 nm. ITO dots with an active-area of 0.25 cm^2 were deposited on the *p* layer for J-V and QE measurements.

The deposition rate of a-Si:H depends on many deposition parameters such as the excitation (VHF or RF) power, gas pressure, and gas dilution ratio. Under a given condition, the most common way to increase the deposition rate is to increase the excitation power. Figure 3 shows the deposition rate of a-Si:H as a function of VHF power. One can see that the deposition rate continues to increase with the VHF power in the range of 9-14 Å/s. The deposition rate is also very sensitive to the gas pressure. In the high pressure regime, increasing the pressure leads to a decrease in the deposition rate. In this study, we focused on deposition rates in the range of 5 to 14 Å/s.

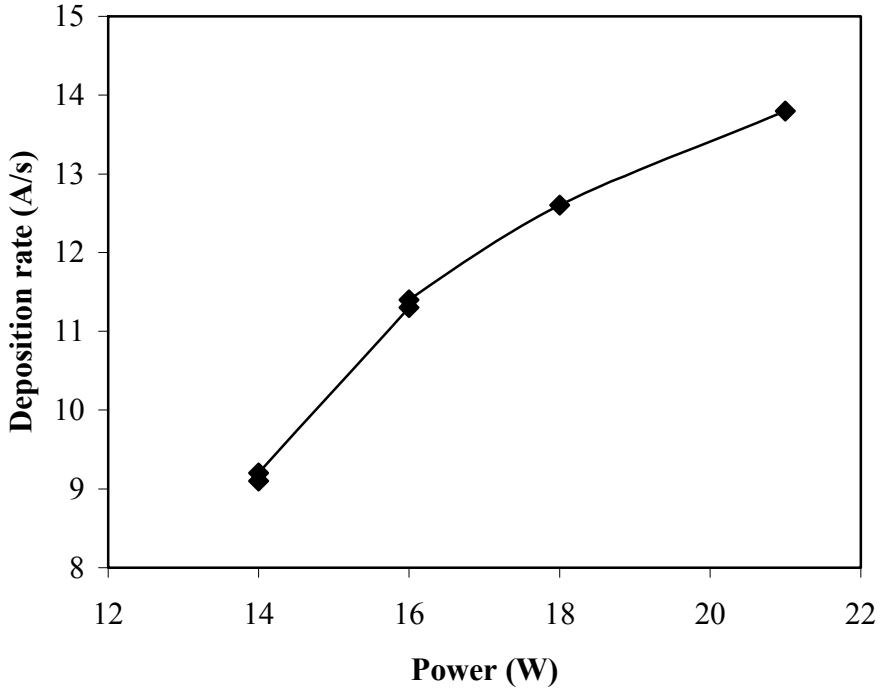

Figure 3. The deposition rate of a-Si:H as a function of VHF power.

Table V lists the J-V characteristics of the cells on both SS and BR substrates, where J_{sc} is obtained from QE measurements. FF_b and FF_r denote the FF obtained from the measurements with weak blue and red lights, respectively. Normally, we believe that the FF_b probes the interface between the *i* and *p* layers, while the FF_r detects the quality of the *i* layer. One can see that the cell performance does not have a strong dependence on the deposition rate. Most cells show a high FF_r, indicating a high quality of the a-Si:H intrinsic layer. The average efficiency is around 7% for the cells on SS and 10% on BR. Compared to the cells on SS, the V_{oc} and FF do not change much for the cells on BR, but the J_{sc} is increased by 40% due to light trapping, which directly improves the cell efficiency. The intrinsic layer thickness in all the cells in the table is in the range of 200-220 nm. By increasing the intrinsic layer thickness to 330 nm, an efficiency of 10.6% (J_{sc}=15.94 mA/cm^2, V_{oc}=0.993 V, and FF=0.674) has been obtained with an a-Si:H single-junction cell on BR deposited at 10 Å/s.

Stability testing has been done on cells made with different deposition rates on SS and BR. The solar cells were light soaked under 100 mW/cm^2 white light at 50 ^{o}C for 1000 hours. As a reference, two a-Si:H cells made with RF at a low rate ~1.0 Å/s (one on SS and one on Ag/ZnO BR) were light-soaked together with the high rate MVHF cells. The results are listed in Tables VI and VII for the cells on BR and on SS, respectively. Figure 4 shows the initial and stable efficiencies as well as the light-induced degradation as a function of the deposition rate. The light-induced degradation rate of the efficiency varies from 15% to 17% for cells on both BR and SS, but it does not show any dependence on the deposition rate. The highest stabilized efficiency of 8.64% has been achieved with an a-Si:H single-junction cell made at 9.3 Å/s on Ag/ZnO back reflector.

Table V. Performance of a-Si:H solar cells made with MVHF on BR and SS substrates. FF_b and FF_r represent the FF measured under weak blue and red lights, respectively. The values of J_{sc} are from QE measurements.

Sample No.	V_{oc} (V)	FF			J_{sc} (mA/cm^2)	Eff (%)	Substrate	Rate (Å/s)	*i* layer time (seconds)
		FF	FF_b	FF_r					
14325	0.983	0.712	0.759	0.753	14.34	10.04	BR	5.2	420
14166	1.000	0.735	0.767	0.749	9.71	7.14	SS		
14324	1.001	0.723	0.763	0.750	13.68	9.90	BR	6.1	300
14139	0.974	0.727	0.765	0.780	9.62	6.81	SS		
14347	0.987	0.702	0.722	0.744	14.67	10.16	BR	9.2	288
14336	0.988	0.710	0.760	0.770	10.36	7.27	SS		
14323	0.993	0.709	0.741	0.741	14.69	10.34	BR	9.3	240
14318	0.978	0.697	0.754	0.763	10.48	7.14	SS		
14346	0.986	0.696	0.716	0.742	14.46	9.92	BR	11.4	222
14335	0.995	0.698	0.764	0.747	10.43	7.24	SS		
14338	0.997	0.704	0.743	0.751	13.68	9.60	BR	11.9	180
14330	0.985	0.714	0.755	0.768	9.96	7.00	SS		
14345	0.984	0.697	0.717	0.742	14.20	9.74	BR	12.6	175
14342	0.986	0.713	0.760	0.767	9.89	6.95	SS		
14348	0.982	0.710	0.717	0.743	14.11	9.84	BR	13.8	156
14333	0.995	0.713	0.769	0.763	9.64	6.84	SS		

Table VI. Stability results of a-Si:H solar cells on Ag/ZnO BR coated SS made by MVHF at high rates. For comparison, a sample (14028) made by RF at a low rate of 1.0 Å/s has been light-soaked with the high rate samples. The thickness for all samples is in the range of 200-220 nm.

Sample No.	State	V_{oc} (V)	FF			J_{sc} (mA/cm^2)	Eff (%)	Rate (Å/s)
			AM1.5	FF_b	FF_r			
14028	Initial	1.020	0.695	0.740	0.719	13.78	9.77	1.0
	Stable	0.998	0.640	0.636	0.653	13.12	8.38	
	Deg(%)	2.2%	7.9%			4.8%	14.2%	
14325	Initial	0.983	0.712	0.759	0.753	14.34	10.04	5.2
	Stable	0.951	0.645	0.677	0.665	13.92	8.54	
	Deg(%)	3.3%	9.4%			2.9%	14.9%	
14324	Initial	1.001	0.723	0.763	0.750	13.68	9.90	6.1
	Stable	0.965	0.668	0.697	0.676	13.05	8.41	
	Deg(%)	3.6%	7.6%			4.6%	15.1%	
14347	Initial	0.987	0.702	0.722	0.744	14.67	10.16	9.2
	Stable	0.958	0.645	0.647	0.667	13.67	8.45	
	Deg(%)	2.9%	8.1%			6.8%	16.8%	
14323	Initial	0.993	0.709	0.741	0.741	14.69	10.34	9.3
	Stable	0.956	0.649	0.644	0.639	13.92	8.64	
	Deg(%)	3.7%	8.5%			5.2%	16.4%	
14346	Initial	0.986	0.696	0.716	0.742	14.46	9.92	11.4
	Stable	0.960	0.655	0.663	0.684	13.49	8.48	
	Deg(%)	2.6%	5.9%			7.2%	14.5%	
14338	Initial	0.997	0.704	0.743	0.751	13.68	9.60	11.9
	Stable	0.959	0.645	0.681	0.672	13.20	8.15	
	Deg(%)	3.8%	8.4%			3.5%	15.1%	
14345	Initial	0.984	0.697	0.717	0.742	14.20	9.74	12.6
	Stable	0.960	0.648	0.656	0.675	13.41	8.34	
	Deg(%)	2.4%	7.0%			5.6%	14.4%	
14348	Initial	0.982	0.710	0.717	0.743	14.11	9.84	13.8
	Stable	0.959	0.659	0.662	0.673	13.34	8.43	
	Deg(%)	2.3%	7.2%			5.5%	14.3%	

Table VII. Stability results of MVHF high rate a-Si:H solar cells on SS. As a reference, a RF low rate a-Si:H cell RF (13899) is also included. The thicknesses for all samples are in the range of 200-220 nm.

Sample No.	State	V_{oc} (V)	FF			J_{sc} (mA/cm^2)	Eff (%)	Rate (Å/s)
			AM1.5	Blue	Red			
13899	Initial	1.014	0.748	0.782	0.760	9.82	7.45	1.0
	Stable	0.974	0.676	0.720	0.677	9.37	6.17	
	Deg. (%)	3.94%	9.63%			4.58%	17.2%	
14166	Initial	1.002	0.732	0.775	0.760	9.71	7.14	5.2
	Stable	0.959	0.661	0.697	0.655	9.41	5.96	
	Deg. (%)	4.3%	9.7%			3.1%	16.5%	
14308	Initial	0.997	0.733	0.782	0.751	9.61	7.07	7.5
	Stable	0.958	0.663	0.721	0.669	9.30	5.91	
	Deg. (%)	3.9%	9.5%			3.2%	16.4%	
14309	Initial	0.979	0.699	0.776	0.752	10.09	6.94	9.0
	Stable	0.944	0.636	0.702	0.636	9.71	5.83	
	Deg. (%)	3.6%	9.0%			3.8%	16.0%	
14318	Initial	0.979	0.702	0.757	0.762	10.48	7.14	9.3
	Stable	0.943	0.626	0.688	0.648	10.05	5.93	
	Deg. (%)	3.7%	10.8%			4.1%	16.9%	
14370	Initial	0.984	0.713	0.756	0.769	10.14	7.11	11.3
	Stable	0.950	0.673	0.687	0.666	9.45	6.04	
	Deg. (%)	3.5%	5.6%			6.8%	15.0%	
14342	Initial	0.986	0.713	0.762	0.765	9.89	6.95	12.6
	Stable	0.952	0.647	0.678	0.670	9.33	5.75	
	Deg. (%)	3.2%	9.3%			5.7%	17.3%	
14333	Initial	0.995	0.713	0.760	0.754	9.64	6.84	13.8
	Stable	0.957	0.650	0.694	0.653	9.17	5.70	
	Deg. (%)	3.8%	8.8%			4.9%	16.7%	

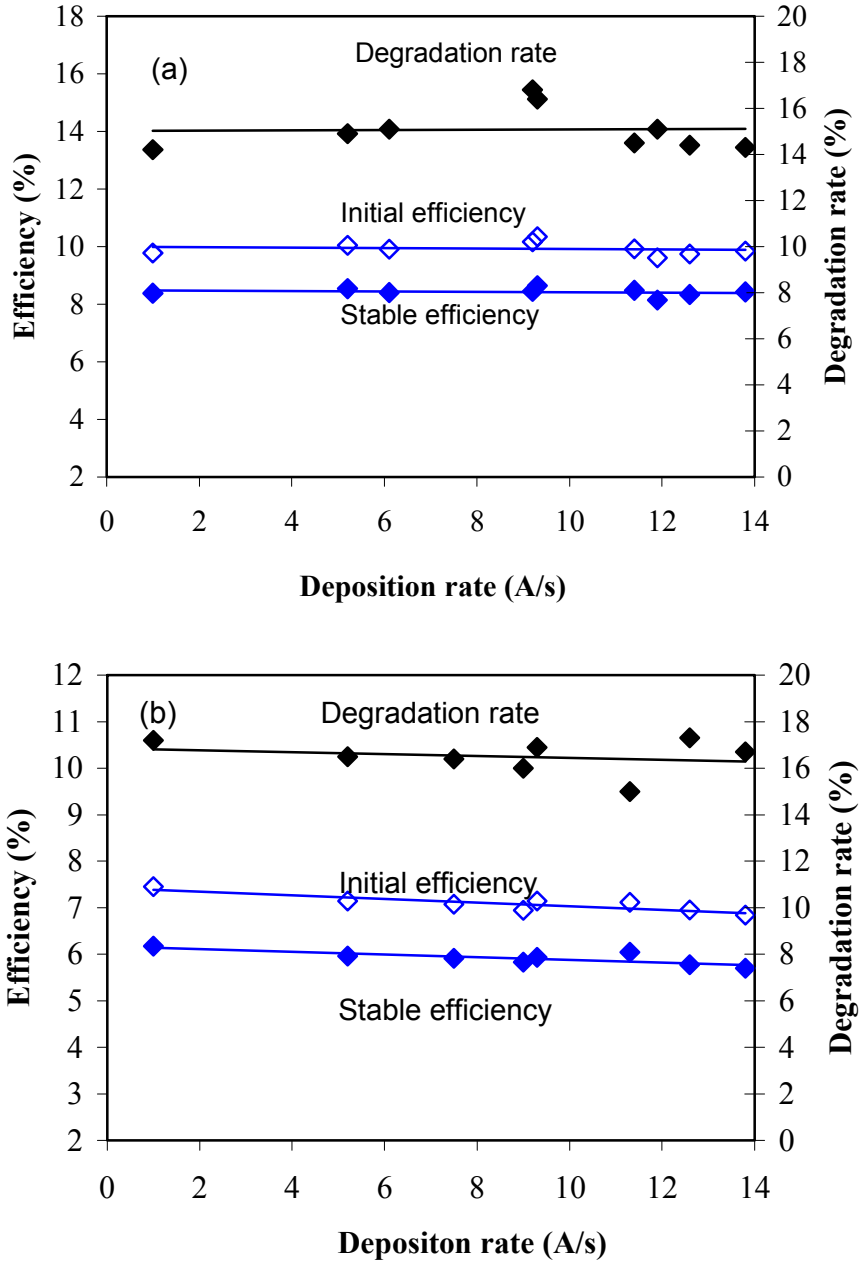

Figure 4. Initial and stable efficiencies of MVHF a-Si:H, as well as their degradation rate, as a function of the deposition rate for the cells on (a) BR and (b) SS.

2.3. High Rate a-SiGe:H Single-Junction Cells Made Using MVHF Technique

A series of a-SiGe:H *n-i-p* single-junction cells was made using MVHF high rate a-SiGe:H intrinsic layer and RF doped layers on stainless steel substrates. The *n/i* and *i/p* buffer layers were made using RF at a low rate of ~1 Å/s. Specular stainless steel substrates were used. It is known that the a-SiGe:H cell performance strongly depends on the Ge/Si ratio in the intrinsic layer and this ratio depends on the deposition rate even if the same GeH_4/SiH_4 ratio in the gas flow rate is used. The reason for the Ge/Si ratio dependence on the deposition rate is due to the difference in the power dependence of the decomposition rate of SiH_4 and GeH_4 in the plasma. In order to simplify the study, the deposition time of the a-SiGe:H intrinsic layer was fixed at 4 minutes, which corresponds to a deposition rate of ~ 10 Å/s. The major techniques to optimize the recipe include: (1) a proper GeH_4 ramping to enhance hole collection, (2) an optimized *i/p* buffer to reduce shunt current and interface recombination, and (3) optimized *p* and *n* layers to reduce series resistance.

Table VIII lists the J-V characteristics of typical a-SiGe:H component cells made at high rates. In this study, we focused on medium bandgap materials, which give an AM1.5 V_{oc} around 0.75 to 0.80 V for the a-SiGe:H component cell in a high efficiency a-Si:H/a-SiGe:H double-junction structure. In order to investigate the long wavelength response and simulate the performance when the a-SiGe:H cell is placed in an a-Si:H/a-SiGe:H double-junction structure, we measured the cell performance under an AM1.5 solar simulator with a 530-nm cut-on filter. From previous experience, a P_{max} of 4 mW/cm^2 is a benchmark for good a-SiGe:H component cell on a stainless steel substrate. In this study, we achieved an active-area P_{max} of 4.4 mW/cm^2 under AM1.5 with a 530-nm cut-on filter. Figure 5 shows the J-V curves and QE spectrum of the optimized a-SiGe:H component cell.

We also studied the stability of the a-SiGe:H component solar cells. The light soaking was made under 100 mW/cm^2 white light with a proper long wavelength pass filter, which results in a J_{sc} in the a-SiGe:H cells similar to the J_{sc} in an a-Si:H/a-SiGe:H double-junction structure. The temperature of the light soaking stage was controlled at 50 °C during the light soaking. After over 1000 hours of light soaking the solar cell performance was stabilized. Table IX lists the initial and stable J-V characteristics measured under an AM1.5 solar simulator with a 530-nm cut-on filter. It appears that the cell performance degrades about 31% on average, which is similar to the light-induced degradation observed in the a-SiGe:H component cells made with RF glow discharge at 3 Å/s.

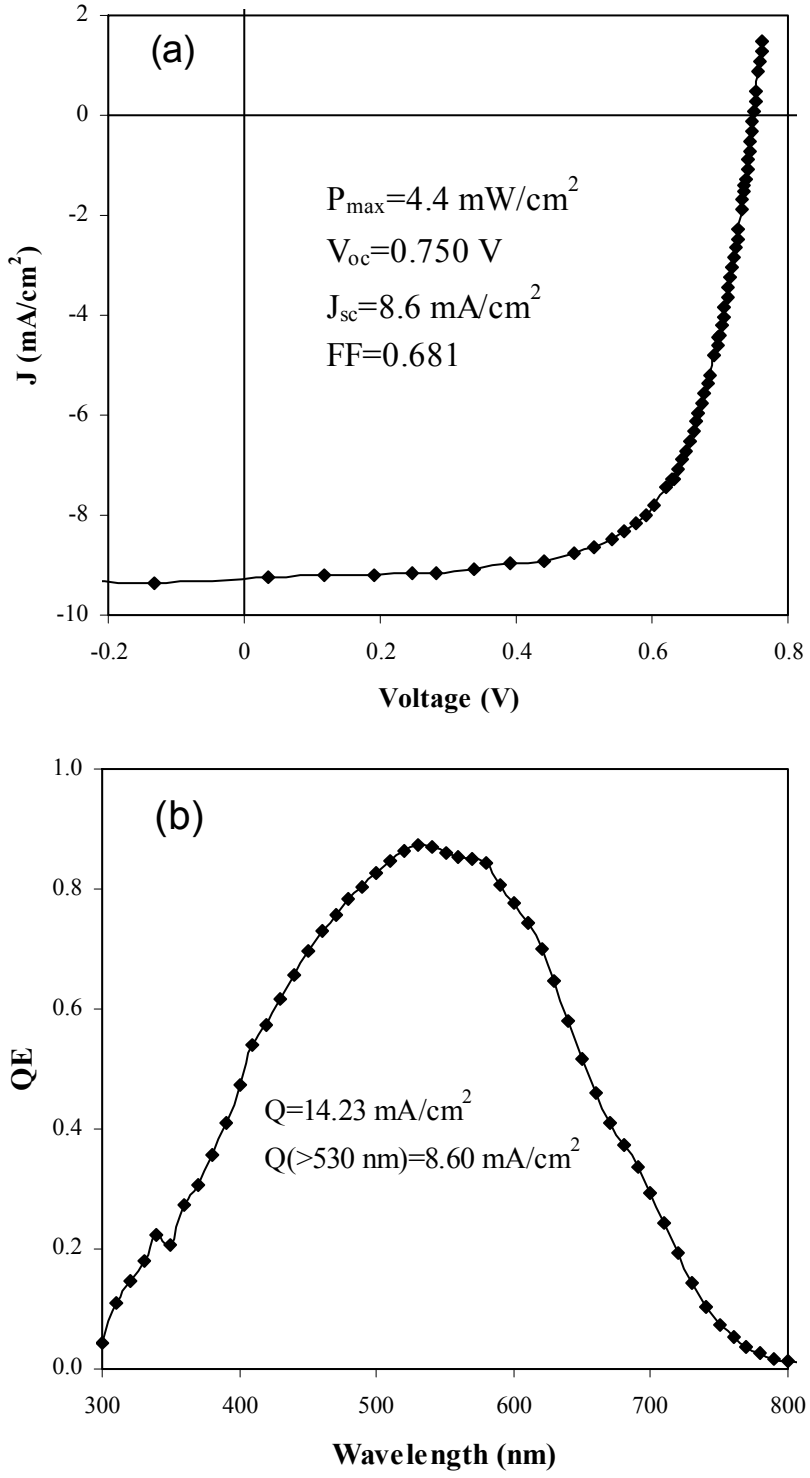

Figure 5. (a) J-V characteristics measured under AM1.5 with a 530 nm cut-on filter and (b) QE spectrum of the best a-SiGe:H middle cell made at 10 Å/s using MVHF.

Table VIII. J-V characteristics of the typical a-SiGe:H component cells made with MVHF at high rates. The intrinsic layer deposition time for all the cells was 4 minutes. The results in parentheses were measured under AM1.5 with a 530 nm cut-on filter.

Sample No.	V_{oc} (> 530 nm) (V)	FF (> 530 nm)	J_{sc} (> 530 nm) (mA/cm^2)	P_{max} (> 530 nm) (mW/cm^2)
14407	0.795(0.775)	0.667(0.696)	13.49(7.82)	7.15(4.22)
14583	0.768(0.751)	0.648(0.671)	14.41(8.66)	7.17(4.36)
14584	0.768(0.750)	0.664(0.681)	14.23(8.60)	7.26(4.39)

Table IX. Stability of a-SiGe:H component cells on SS made by MVHF at a deposition rate of ~ 10 Å/s. The light soaking was carried out under 100 mW/cm^2 white light with a 515 nm cut-on filter at 50 ^oC for 1095 hours. The cells were measured under an AM1.5 solar simulator with a 530-nm cut-on filter at 25 ^oC.

Sample No.	Status	V_{oc} (V)	FF	J_{sc} (mA/cm^2)	P_{max} (mW/cm^2)
14382	Initial	0.784	0.693	7.67	4.17
	Stable	0.728	0.553	7.06	2.84
	Degradation (%)	7.1%	20.2%	8.0%	31.9%
14395	Initial	0.780	0.677	7.67	4.05
	Stable	0.722	0.542	7.05	2.76
	Degradation (%)	7.4%	19.9%	8.1%	31.9%
14407	Initial	0.774	0.682	7.82	4.13
	Stable	0.718	0.545	7.36	2.88
	Degradation (%)	7.2%	20.1%	5.9%	30.3%
14397	Initial	0.785	0.675	7.50	3.97
	Stable	0.727	0.538	6.92	2.71
	Degradation (%)	7.4%	20.3%	7.7%	31.7%

2.4. a-Si:H/a-SiGe:H Double-Junction Solar Cells Made With MVHF at High Rates

Having optimized the a-Si:H top and a-SiGe:H bottom cells, we proceeded to combine them to make a-Si:H/a-SiGe:H double-junction solar cells on Ag/ZnO coated stainless steel substrates. The deposition time for both the a-Si:H intrinsic layer in the top cell and a-SiGe:H intrinsic layer in the bottom cell was fixed at 4 minutes. The J-V characteristics of typical double-junction cells are listed in Table X. An initial active-area efficiency of 11.7% has been achieved. The J-V curves and QE spectrum of the best a-Si:H/a-SiGe:H double-junction cell are plotted in Fig. 6.

2.5. Summary

In summary, we have found that the MVHF-deposited a-Si:H solar cells showed good initial efficiency and stability. The most important result is that the cell performance and stability do not depend on the deposition rate up to 14 Å/s. This phenomenon is quite different from the cells made using RF at high rates. The degradation rate of the RF-cells usually increases with the deposition rate. We have also optimized the a-SiGe:H component cells at high deposition rates on SS substrate. An active-area P_{max} of 4.4 mW/cm^2 has been achieved under AM1.5 with a 530 nm cut-on filter. The light-induced degradation of the a-SiGe:H component cells is about 31%, which is similar to the cells made with RF glow discharge at 3 Å/s. By combining this cell with an optimized high rate a-Si:H top cell, we have made an a-Si:H/a-SiGe:H double-junction cell on Ag/ZnO coated SS with an initial active-area efficiency of 11.7%.

Table X. J-V characteristics of the a-Si:H/a-SiGe:H double-junction cells made at high rates. The deposition time for both top and middle cell intrinsic layers was 4 minutes.

Sample No.	V_{oc} (V)	FF	QE (mA/cm^2)			P_{max} (mW/cm^2)
			Top	Bottom	Total	
14520	1.719	0.717	9.50	10.94	20.44	11.71
14530	1.696	0.664	10.23	10.16	20.39	11.44
14534	1.700	0.679	9.78	10.48	20.26	11.29

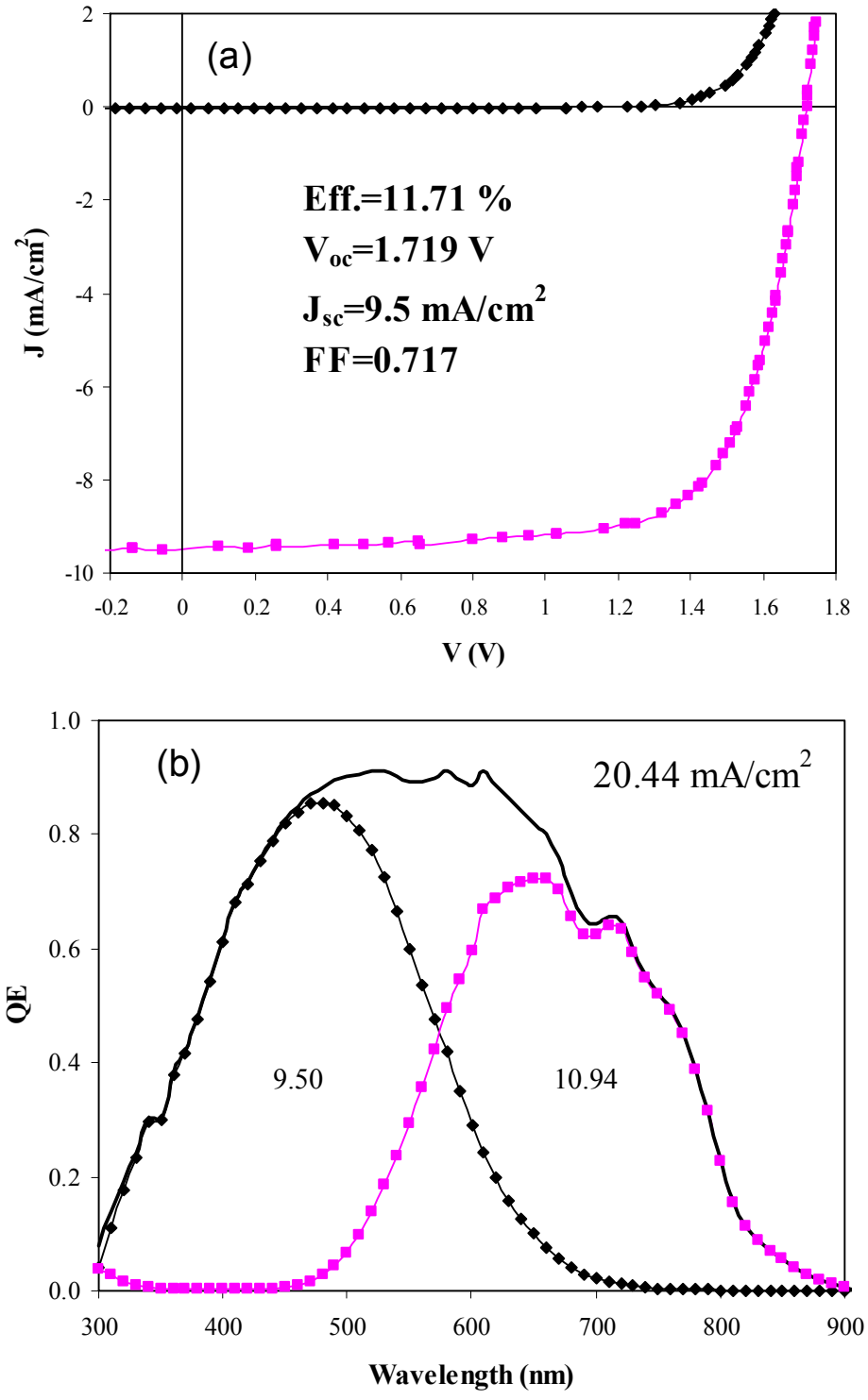

Figure 6. (a) J-V characteristics and (b) QE spectrum of an a-Si:H/a-SiGe:H double-junction cell made at 10 Å/s using MVHF.

3. High Efficiency Hydrogenated Amorphous Silicon Based Triple-Junction Solar Cells Incorporating Nanocrystalline Silicon

3.1. Introduction

A world record stable cell efficiency of 13.0% was achieved previously by using a-Si:H and a-SiGe:H alloys in a spectrum-splitting, triple-junction structure [11]. This technology has been used in United Solar's two ~30 MW production lines [12] and will be used in the next 60 MW plant in Greenville, Michigan. In recent years, nc-Si:H has attracted remarkable attention due to its superior long wavelength response and reported improved stability. Significant progress has been made resulting in cell efficiency approaching 15% [13] and module efficiency of over 13% [14]. In our laboratory, we have focused on the development of nc-Si:H solar cells and explored the possibility of substituting nc-Si:H for the a-SiGe:H middle and bottom cells in our triple-junction structure. We have carried out various studies for improving the nc-Si:H cell performance, stability, and deposition rate [8-10, 15,16]. A hydrogen dilution profiling technique has been developed and shown to be an effective way of controlling the nc-Si:H material structure and improving the cell performance [15]. Using this technique, we have recently reported an initial active-area efficiency of 14.6% for an a-Si:H/a-SiGe:H/nc-Si:H triple-junction structure [16]. In Phase I of this project, we have focused on the optimization of nc-Si:H solar cells at high rates and used the optimized nc-Si:H cell in a-Si:H/a-SiGe:H/nc-Si:H and a-Si:H/nc-Si:H/nc-Si:H triple-junction structures. We have achieved an initial active-area efficiency of 15.1% using an a-Si:H/a-SiGe:H/nc-Si:H triple-junction structure. We concentrated on three areas: First, we have carried out a systematic study to understand the correlation of material structures and cell performance as well as the stability in nc-Si:H solar cells. Second, we have optimized the cell structure by optimizing the *i/p* buffer layer and its effect on cell performance and stability. Third, we have used the optimized parameters to attain the highest multi-junction cell efficiency.

3.2. Correlation of Material Structure and Metastability in nc-Si:H

One of the advantages of nc-Si:H over a-SiGe:H in multi-junction solar cells is the improved stability after prolonged light soaking. Previously, several groups reported that there was no light-induced degradation in nc-Si:H solar cells [17-19]. However, we found that nc-Si:H single-junction cells made in our laboratory showed light-induced degradation in the range of 3% to 15% [20-22]. Surprisingly, the light-induced degradation was increased by applying a reverse electrical bias during light soaking [21,22], contrary to the decreased degradation observed in a-Si:H solar cells. We proposed a back-to-back micro-diode model to explain the enhanced light-induced degradation by a reverse bias in the nc-Si:H solar cells. A wavelength dependent light-soaking study showed that the light-induced degradation mainly occurs in the amorphous and/or grain boundary regions [20]. Meanwhile, several recent reports show that the light-induced degradation is dominated by the amount of amorphous component in the nc-Si:H intrinsic layer [23,24]. On the other hand, nc-Si:H cells made near the nanocrystalline/amorphous transition, which usually have a large volume fraction of amorphous component, show the best performance [25]. In order to improve the nc-Si:H cell performance and stability at the same time, a better understanding of the factors determining the metastability is essential.

We have made significant progress in understanding the mechanism of light-induced degradation in nc-Si:H solar cells [20-22]. We have also tried to improve the stability of the nc-Si:H cell by optimizing the deposition process and device design. As previously reported, hydrogen dilution profiling is an effective method of controlling the nanocrystalline evolution during the deposition of nc-Si:H and improves the initial solar cell performance [15].

In Phase I of this project, we have systematically studied the metastability of nc-Si:H solar cells made with various hydrogen dilution profiles and correlated the results to the material structural properties. Using this knowledge, we have further optimized the material structure and improved the cell performance and stability.

Most of the nc-Si:H single-junction solar cells reported here were deposited using a multi-chamber glow discharge system with RF excitation for the doped layers and a modified VHF (MVHF) technique for the intrinsic nc-Si:H layers. Some of the cells have an RF deposited nc-Si:H film as the intrinsic layer. The nanostructure evolution in the nc-Si:H intrinsic layer was controlled by hydrogen dilution profiling with decreasing dilution ratio during the deposition. The profiling was achieved both by continuously changing the dilution (dynamic profiling) and by changing dilution in three discrete steps during deposition (step profiling). Light soaking was carried out with a 100 mW/cm^2 white light at 50 °C under the open circuit condition for over 1000 hours. The J-V characteristics were measured under an AM1.5 solar simulator at 25 °C. QE spectra were measured from 300 nm to 1100 nm at room temperature. The material structure of the intrinsic layer was directly measured on the solar cells using Raman spectroscopy with different excitation wavelengths.

Table XI lists the J-V characteristics of two sets of nc-Si:H single-junction solar cells at their initial and stable states. The intrinsic nc-Si:H layers in the first set (the first three cells) were deposited using RF. MVHF was used for the nc-Si:H intrinsic layer deposition in the second set

Table XI. Initial (A) and stable (B) performance of nc-Si:H cells. C refers to the percentage of light-induced change.

Run #	Dep. Method	H Dilution	State	Eff (%)	J_{sc} (mA/cm^2)	V_{oc} (V)	FF
10514	RF	Constant	A	7.85	23.06	0.499	0.682
			B	6.73	22.44	0.470	0.638
			C	-14.3%	-2.7%	-5.8%	-6.5%
10521	RF	Constant	A	7.21	23.03	0.461	0.679
			B	6.12	22.65	0.426	0.634
			C	-15.1%	-1.7%	-7.6%	-6.6%
10505	RF	Dynamic Profiling	A	7.56	22.76	0.520	0.638
			B	7.30	22.91	0.517	0.616
			C	-3.5%	+0.7%	-0.6%	-3.4%
12085	MVHF	Step Profiling	A	6.62	21.76	0.479	0.635
			B	6.06	21.65	0.470	0.596
			C	-8.5%	-0.5%	-1.9%	-6.1%
13324	MVHF	Dynamic Profiling	A	6.75	23.89	0.490	0.577
			B	6.52	23.16	0.481	0.585
			C	-3.4%	-3.1%	-1.8%	+1.4%
13348	MVHF	Dynamic Profiling	A	7.82	22.72	0.524	0.657
			B	7.72	21.85	0.527	0.670
			C	-1.3%	-3.9%	+0.6%	+2.0%

(the last three cells). The first two RF cells using a constant hydrogen dilution during the intrinsic layer deposition show a large light-induced degradation of 14-15% in efficiency, mainly due to reductions in open-circuit voltage (V_{oc}) and fill factor (FF). The third cell, with an optimized hydrogen dilution profiling, shows only a 3.5% light-induced degradation. Similarly, for the MVHF cells, the cell with a step hydrogen dilution profiling shows an 8.5% light-induced degradation, which is somewhat lower than the RF cells with constant hydrogen dilution, but is still much larger than the two dynamically profiled cells. The V_{oc} and FF in the MVHF cell (13348) with an optimized hydrogen dilution profiling did not degrade after prolonged light soaking; in fact, the FF of this cell was slightly improved.

In order to obtain a better understanding of the mechanism of the light-induced degradation of nc-Si:H solar cells and its relation to the deposition process as well as material structures, Raman measurements were carried out directly on the six solar cells. Figure 7 shows the Raman spectra of sample 10521 (made with RF) excited with a green (532 nm) laser and a red (633 nm) laser. The green light probes the material structure in the top layer near the *i/p* interface, while the red light reveals the information from the bulk of the intrinsic layer. One can see that the crystalline volume fraction is higher in the top layer (measured with the green laser) near the *i/p* interface than in the bulk. This result is consistent with the normally observed nanocrystalline evolution with thickness. Figure 8 shows the Raman spectra of sample 13348 (made with MVHF) excited with the green laser and the red laser. From the two spectra, one can clearly see that in this sample, the region near the *i/p* interface has lower crystalline volume fraction than the bulk of the intrinsic layer. We deconvoluted the Raman spectra into different components of amorphous LA (~310 cm^{-1}), LO (~380 cm^{-1}), TO (~480 cm^{-1}), intermediate (~500 cm^{-1}), and crystalline (~520 cm^{-1}) modes. Table XII lists the parameters of the amorphous TO, intermediate, and the crystalline modes. It is common to determine the crystalline volume fraction from the area under each deconvoluted curve with a correction factor for the grain size dependence of the Raman cross-section [26-28]. For simplicity, we only present the ratio of areas for each component. To emphasize the key points, Fig. 9 plots (upper panel) initial and stable efficiencies with a comparison to (lower panel) the fractions of each Raman component obtained by deconvolution of the Raman spectra measured using the green and red lasers. From Table XII and Fig. 9, three important phenomena are observed. First, the crystalline volume fraction (the narrow peak at ~520 cm^{-1}) is higher for the green laser than the red laser in the samples with constant hydrogen dilution (sample 10514), as normally observed in the nanocrystalline evolution with thickness. The optimized hydrogen dilution profiling (samples 10505 and 13348) reversed this trend and resulted in a lower crystalline volume fraction in the region near the *i/p* interface as previously reported [15]. Second, the stable cells have lower crystalline volume fractions than those with high light-induced degradation, especially at the *i/p* interface region probed by the green light. Third, although the crystalline peak is smaller in the stable cells than in the less stable samples, the intermediate range peak is larger, becomes broader, and shifts to lower wavenumbers.

From the three observations, we believe that the light-induced degradation in nc-Si:H solar cells does not necessarily increase (instead, it decreases in our solar cells) with increasing amorphous volume fraction. Also, it appears that the stable cells have a relatively large and broad intermediate Raman peak. It is reasonable to speculate that this intermediate peak plays a role in the metastability. The origin of the intermediate Raman peak could be due to the intermediate range order [29,30], such as the linear-like structure in high hydrogen diluted a-Si:H, and/or from grain boundaries [26-28]. The observed improved stability of high hydrogen diluted a-Si:H was suggested to be due to the intermediate range order [29,30]. At this time, we believe that both

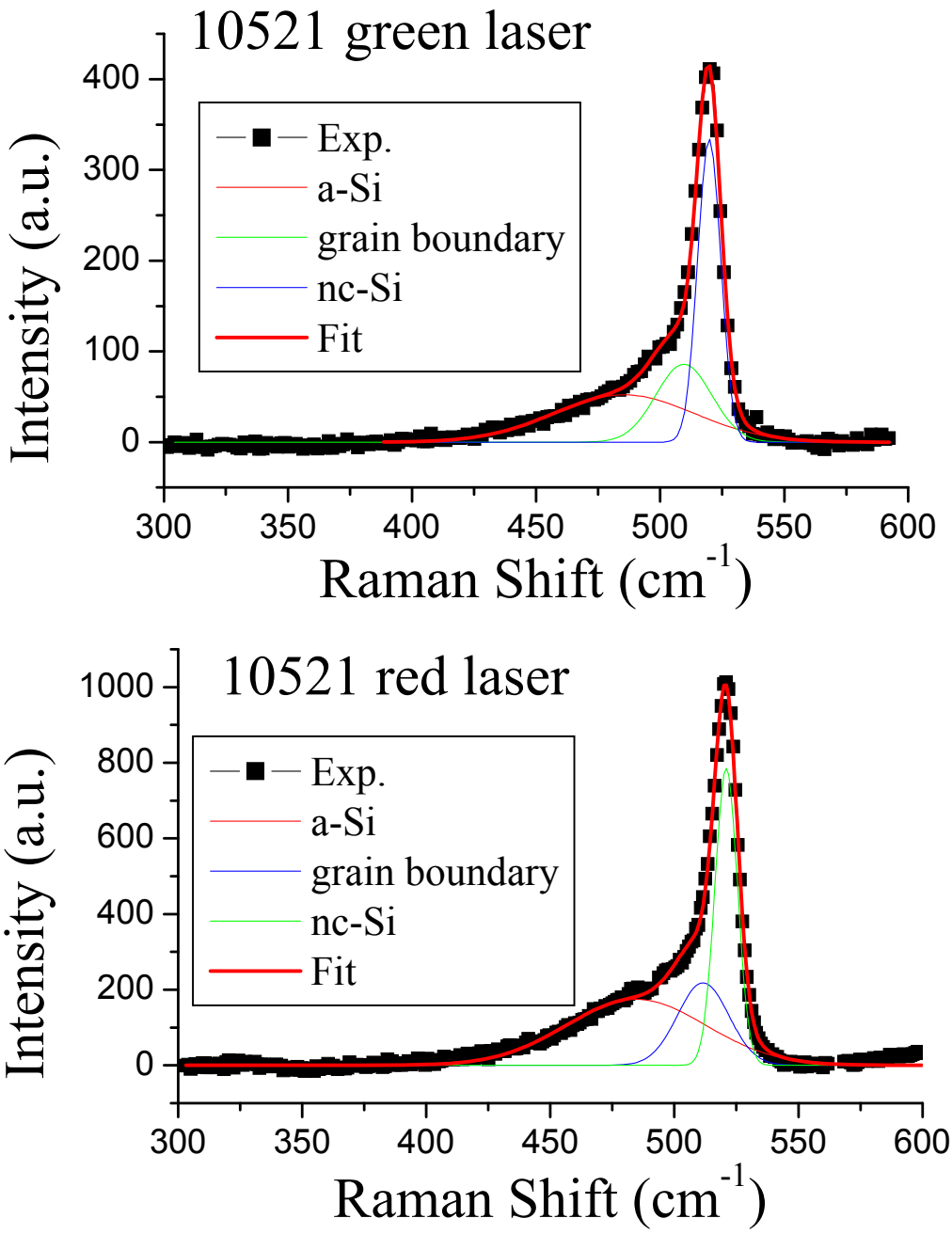

Figure 7. Raman spectra and their deconvolutions of cell 10521 (made with RF) excited with (upper) a green laser and (lower) a red laser.

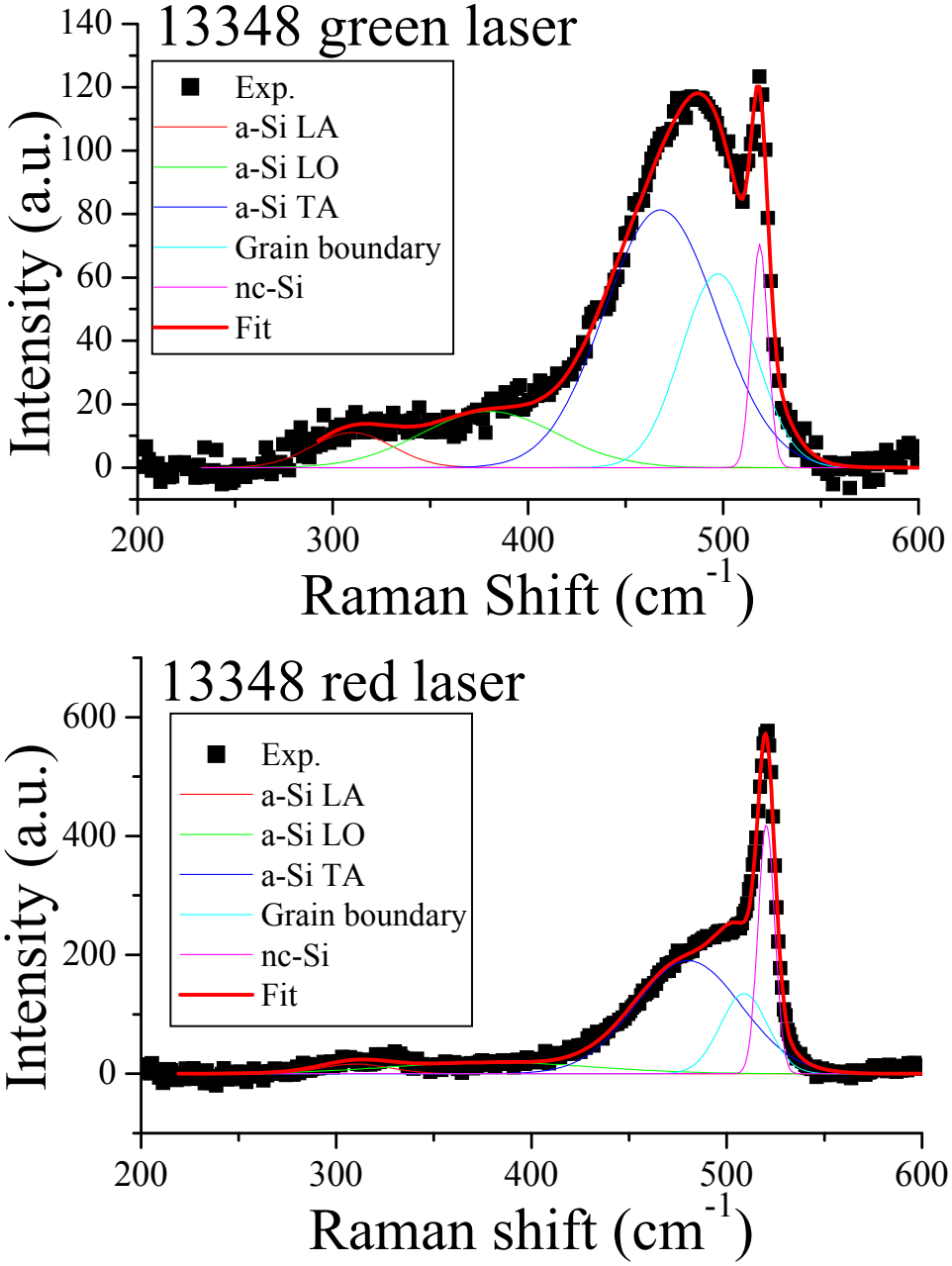

Figure 8. Raman spectra and their deconvolutions of cell 13348 (made with MVHF) excited with (upper) a green laser and (lower) a red laser.

Table XII. Raman deconvolution data for six nc-Si:H solar cells measured with green (532.0 nm) and red (632.8 nm) lasers. a, i, and c denote the three peaks corresponding to the amorphous TO, intermediate, and the crystalline TO peaks. p, w, and f denote the peak position, width, and area percentage of each peak. R is the crystalline volume fraction with the crystalline and intermediate components.

Run #	λ (nm)	a			i			c			R (%)
		p_a (cm^{-1})	w_a (cm^{-1})	f_a (%)	p_i (cm^{-1})	w_i (cm^{-1})	f_i (%)	p_c (cm^{-1})	w_c (cm^{-1})	f_c (%)	
10514	532.0	469.1	78.7	45.1	501.2	37.8	27.3	517.1	10.2	27.6	54.9
	632.8	481.6	65.7	59.0	510.7	21.5	16.7	519.1	10.3	24.3	45.8
10521	532.0	483.7	65.5	36.5	508.4	27.6	24.7	518.6	10.2	38.9	63.6
	632.8	485.4	65.6	46.1	511.6	24.3	21.2	520.9	10.3	32.8	54.0
10505	532.0	457.5	70.1	45.2	486.8	53.9	50.9	514.2	13.1	3.9	54.8
	632.8	471.3	64.8	57.0	499.4	41.2	26.5	518.1	11.2	16.5	43.0
12085	532.0	479.4	69.9	56.5	505.5	29.1	17.1	518.6	11.6	26.4	43.5
	632.8	483.5	63.8	49.9	509.7	24.3	19.6	520.0	11.2	30.5	50.1
13324	532.0	480.8	67.0	58.0	508.4	26.1	18.4	518.6	8.7	23.5	41.9
	632.8	484.4	65.6	47.3	511.6	25.2	23.9	520.9	9.3	28.8	52.7
13348	532.0	467.7	68.5	61.8	496.8	43.6	30.4	518.6	10.2	7.7	38.1
	632.8	480.7	63.8	60.1	508.8	29.0	19.1	520.0	10.3	20.8	39.9

assignments are possible, depending on the structure of the material. In our case, when the nc-Si:H intrinsic layer was deposited under a controlled hydrogen dilution profiling, although a significant amount of small grains was incorporated in the material, they were not allowed to grow into larger grains. These small grains may not contribute to the sharp crystalline Raman peak, but can contribute to the intermediate peak. From the correlation between the solar cell stability results and the Raman analyses, we speculate that our stable nc-Si:H cells have a large amount of small grains and intermediate range order, especially near the *i/p* interface.

The increase of the intermediate order along the growth direction is also an important feature. It is known that the *i/p* interface is the dominant junction in an *n-i-p* (or *p-i-n*) structure [31]. The small grains with a reasonable amount of amorphous component in the *i/p* interface region may provide a good grain boundary passivation and a compact material structure, which reduce defect density and any impurity diffusion. As a result, the V_{oc} of the cell is improved. The high crystalline volume fraction in the bulk of the nc-Si:H intrinsic layer, especially in the *n/i* region, ensures sufficient long wavelength absorption resulting in a high short-circuit current density (J_{sc}); it also provides high mobility paths for carrier transport resulting in an improved fill factor (FF). One may suspect that the amorphous component in the *i/p* region would cause extra light-induced degradation. In fact, it is true that the J_{sc} in some hydrogen-dilution profiled nc-Si:H cells, such as #13324 and #13348 in Table XII, decreases due to the short wavelength response. The reduced short wavelength response results from the recombination in the amorphous phase near the *i/p* interface and can be annealed back at a high temperature. We also observed a loss of FF measured under blue light (not shown). The FF measured under white light is not significantly affected because the transport of carriers generated in the bulk of the intrinsic layer goes through the nanocrystalline path with well passivated grain boundaries. From this result, we believe that a decrease of crystalline volume fraction and grain size along the growth direction in a nc-Si:H *n-i-p*

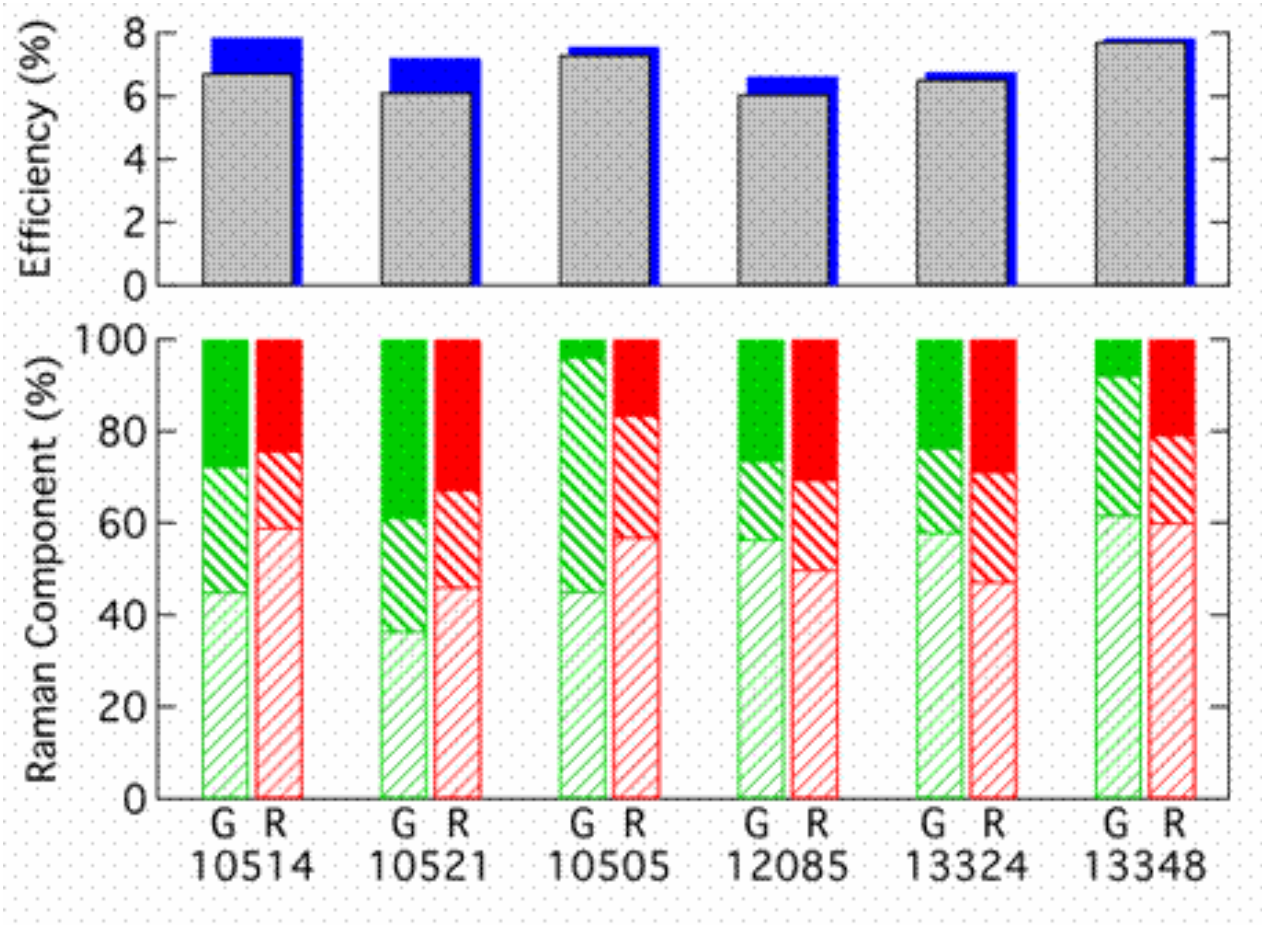

Figure 9. The upper plot shows the initial (back block) and stable (front block) efficiencies of nc-Si:H solar cells. The lower plot shows the fractions of different Raman components of amorphous (lower block), intermediate (middle block), and crystalline (upper block) modes in nc-Si:H cells measured with 532-nm (G) and 633-nm (R) lasers.

structure near the *i/p* interface is beneficial for the cell performance and stability. This feature can be obtained by reducing hydrogen dilution during the nc-Si:H deposition in the *n-i-p* structure and can also occur naturally when the nc-Si:H intrinsic layer in a *p-i-n* structure is deposited on the *p* layer [4].

Three conclusions have been drawn about the metastability of nc-Si:H solar cells. First, the amorphous component is not necessarily the determining factor for the light-induced degradation in nc-Si:H solar cells. Second, smaller grains and intermediate range order may provide a better grain boundary passivation, and hence improve the cell stability. Third, a decrease of crystalline volume fraction along the growth direction in an *n-i-p* structure, especially near the *i/p* interface, can improve the cell performance and the stability. This has been accomplished by an optimized hydrogen dilution profile.

3.3. nc-Si:H Solar Cells With Different Thicknesses of the Intrinsic and *i/p* Buffer Layers

We previously reported [8] that as the intrinsic layer thickness increases, V_{oc} drops more significantly in nc-Si:H cells than in a-Si:H cells. We attributed this to the fact that the crystalline volume fraction increases with increasing thickness. We also found that the nc-Si:H cell performance strongly depends on the *i/p* buffer layer [8]. Without a proper buffer layer, the nc-Si:H cell shows a poorer FF and a smaller V_{oc}, which, in turn, leads to low conversion efficiency. Recently, we found that the metastable behavior after prolonged light soaking in nc-Si:H solar cells is different from a-Si:H cells in many cases. Although this is mainly caused by the difference in the intrinsic material properties, the interface also has certain potential influence on the metastability. In Phase I of this project, we carried out a systematic study of the effects of the intrinsic and *i/p* buffer layer thicknesses on nc-Si:H cell performance and stability. To avoid the microstructure evolution with thickness as mentioned before, the hydrogen dilution profiling technique [15] has been used so that the intrinsic layers in all the cells maintain similar crystalline volume fraction along the growth direction. The results show that both the cell performance and the stability are related to the intrinsic and *i/p* buffer layer thicknesses.

nc-Si:H *n-i-p* single-junction solar cells were deposited using a multi-chamber glow discharge system with RF chambers for the doped layers and a MVHF chamber for the intrinsic layers at a deposition rate of ~ 3-5 Å/s. The same hydrogen dilution profile was used for all the intrinsic layer depositions. The same *n/i* buffer and seeding layers were used for all the samples. The samples with different intrinsic layer thicknesses were made by controlling intrinsic layer deposition time. The a-Si:H *i/p* buffers were made with RF glow discharge at a deposition rate of ~ 1 Å/s. For comparison, high rate a-Si:H cells with different intrinsic layer thicknesses were also made with MVHF at a deposition rate of ~ 6 Å/s. Both nc-Si:H and a-Si:H cells were deposited on Ag/ZnO coated stainless steel substrates. The material structure of the intrinsic layer was directly measured on the cells with no *i/p* buffer layer using Raman spectroscopy with a green light (532 nm) excitation. Light soaking was carried out under 100 mW/cm^2 of white light at 50 ^{o}C under the open circuit condition for 1000 hours. Dark J-V characteristics of the cells were measured in a vacuum chamber using a programmable multi-meter at a controlled temperature.

Table XIII lists the J-V characteristics of nine nc-Si:H single-junction solar cells with different intrinsic and *i/p* buffer layer thicknesses. The same hydrogen dilution profile was used for all the nc-Si:H intrinsic layer depositions. The different intrinsic layer thicknesses were obtained by controlling deposition time as listed in column two. For each intrinsic layer thickness, three different thicknesses of a-Si:H *i/p* buffers with the deposition times of 0, 3, and 7 minutes (corresponding to thicknesses of 0, 180, and 420 Å) were added to study the effect of buffer layer thickness. From Table XIII, the following observations are made. For the effect of the intrinsic layer thickness, we found that the FF decreases and the J_{sc} increases with increasing intrinsic layer thickness. The V_{oc} does not change much with intrinsic layer thickness for the cells with zero and 3-minute *i/p* buffer layers. However, for the cells with a 7-minute *i/p* buffer layer, the V_{oc} decreases noticeably with an increase in the intrinsic layer thickness. Also, the conversion efficiency increases with the intrinsic layer thickness. For the effect of the *i/p* buffer layer thickness, three points can be made. First, the V_{oc} increases with increasing *i/p* buffer layer thickness. Second, the FF does not improve by adding the *i/p* buffer layer. For the thin cells, the FF is even reduced. Third, the *i/p* buffer layer has a greater effect on the thin cells than the thick ones. For example, when the *i/p* buffer layer thickness was increased from 0 to 7 minutes, the

Table XIII: J-V characteristics of nine nc-Si:H single-junction solar cells on Ag/ZnO substrate with different thicknesses of the intrinsic and *i/p* buffer layers.

Sample No.	Time (i) (min)	Time (i/p) (min)	V_{oc} (V)	FF	J_{sc} (mA/cm^2)	P_{max} (mW/cm^2)
14098	7	0	0.463	0.714	14.54	4.81
14099	15	0	0.455	0.641	18.71	5.46
14100	30	0	0.455	0.586	22.49	6.00
14101	7	3	0.481	0.700	14.18	4.77
14111	15	3	0.473	0.642	18.78	5.70
14112	30	3	0.473	0.590	22.87	6.38
14113	7	7	0.532	0.677	16.00	5.76
14114	15	7	0.491	0.622	19.73	6.03
14106	30	7	0.483	0.590	22.82	6.50

V_{oc} increased from 0.463 to 0.532 V for the cells with a 7-minute intrinsic layer, which is significantly larger than the increase from 0.455 to 0.483 V for the cells with a 30-minute intrinsic layer. This phenomenon is even more pronounced in the FF. For the cells with a 7-minute intrinsic layer, the FF is reduced from 0.714 to 0.677 when the *i/p* buffer layer is increased from 0 to 7 minutes. However, for the cells with a 30-minute intrinsic layer, the FF is not sensitive to the *i/p* buffer layer thickness.

As mentioned previously, to control the effect of microstructure evolution on the cell performance, we have used the hydrogen dilution profiling technique in the intrinsic layer deposition to keep the crystalline volume fraction constant in the material along the growth direction. To confirm this, Raman spectroscopy measurements were made on the cells with different intrinsic layer thicknesses by using the green laser (532 nm). In order to avoid the potential influence of the a-Si:H *i/p* buffer on measurement results, the cells with no *i/p* buffer layer (samples 14098, 14099, 14100) were selected for the Raman measurements. Figure 10 (a) shows the Raman spectra for the three samples. One can clearly see that the three cells have very similar crystalline volume fractions. For a detailed analysis, we deconvoluted the Raman spectra into three components of amorphous TO (~ 480 cm^{-1}), intermediate (~ 500 cm^{-1}), and crystalline (~520 cm^{-1}) modes using three Gaussian functions as shown in Fig. 10 (b). The results are summarized in Table XIV. The crystalline volume fraction listed in the table is simply defined as the ratio of the areas of the crystalline and the intermediate modes to the total. The crystalline volume fractions for the cells with 7, 15, and 30 minutes of intrinsic layers are

Table XIV. Deconvolution results of the Raman spectra, where s, p, w, and f denote the area, peak position, width, and percentage of each component, respectively. R represents the ratio of the areas of the c-Si and intermediate peaks to the total areas of the three peaks.

Sample No.	amorphous				intermediate				crystalline				R (%)
	s_a	p_a	w_a	f_a(%)	s_i	p_i	w_i	f_i(%)	s_c	p_c	w_c	f_c(%)	
14098	18.1	481	86	53.4	6.2	505	29	18.3	9.6	520	11	28.3	46.6
14099	12.7	479	70	43.2	6.9	507	29	23.5	9.8	520	13	33.3	56.8
14100	10.8	478	69	39.1	6.8	507	29	24.6	10.0	520	13	36.3	60.9

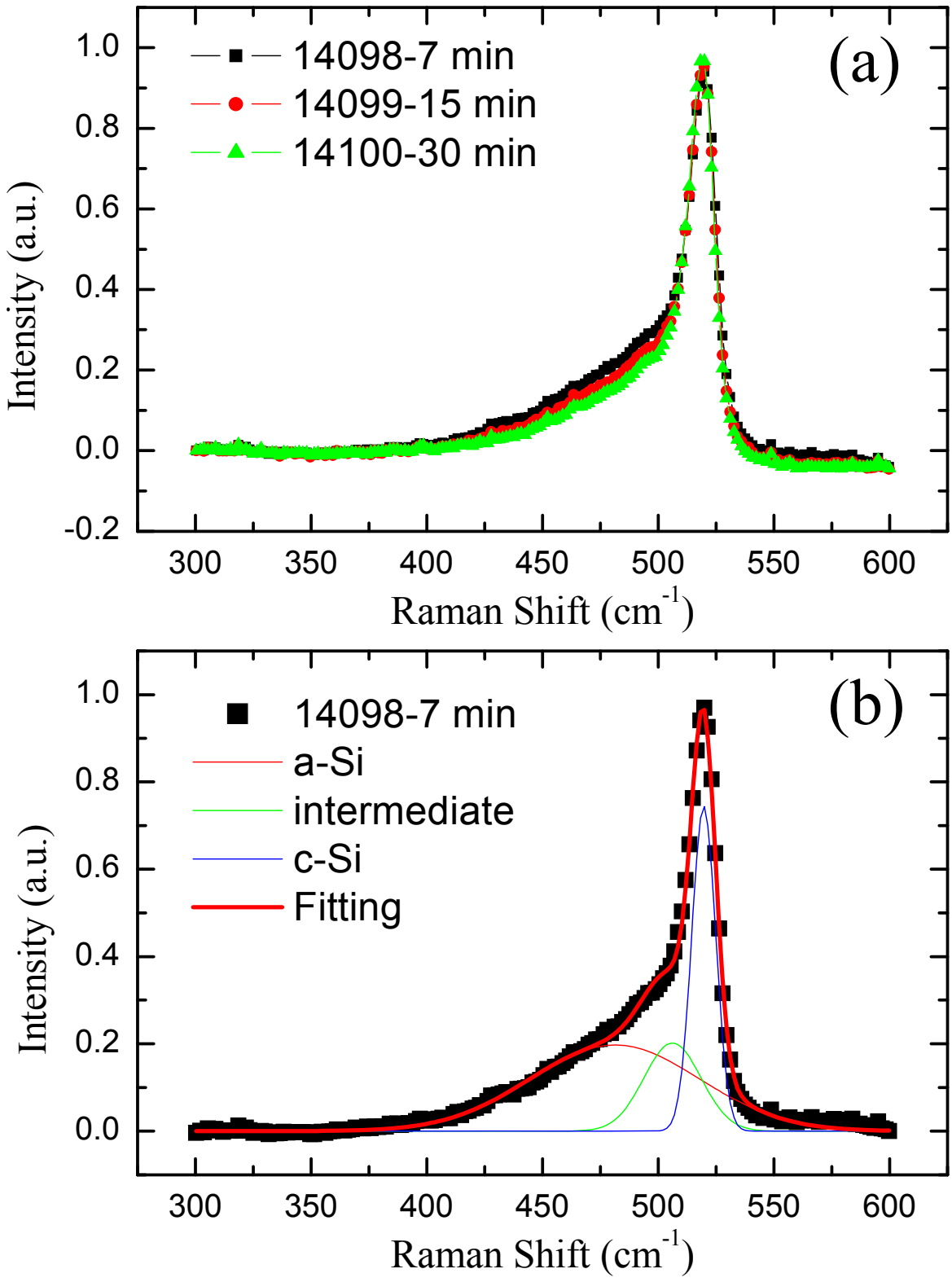

Figure 10. (a) Comparison of Raman spectra for the samples with different intrinsic thicknesses and with no *i/p* buffer, (b) an example of a Raman spectrum deconvolution.

.

46.6%, 56.8%, and 60.9%, respectively. We noted that the volume fraction in the thicker cell is still slightly higher than in the thinner one.

Dark J-V measurement is a useful tool in studying the recombination mechanism in a-Si:H based solar cells. An ideal solar cell follows the typical diode characteristics of $J=J_0[exp(qV/nKT)-1]$, where J_0 is the reverse saturated current density, q the unit charge, T the measurement temperature, k the Boltzmann constant, and n the diode quality factor. By studying the dark J-V characteristics and examining the deviation of experimental results from the diode characteristics, one can examine the shunt current and the recombination mechanism of the carriers in solar cells. In this study, we used the dark J-V measurement to study the nine nc-Si:H solar cells. The results are plotted in Fig. 11. One can see that the dark current density reduces with the increased *i/p* buffer layer thickness. The cells with a thinner intrinsic layer show a larger reduction in the dark current density. Moreover, we found that the cells with no *i/p* buffer layer have a high shunt current density. With the *i/p* buffer layer thickness increased, the shunt current density is continually reduced.

For the cells with a 7-minute *i/p* buffer, the shunt current density becomes minimized and the dark J-V curves basically follow the diode characteristics as shown in Fig. 11 (d). By fitting the data of these three samples with the diode characteristics, we obtained J_0 and n, as listed in Table XV. One can see that the diode quality factors are very similar, which means that the carrier recombination mechanism is the same for the samples. The saturated current is increased by increasing the thickness of the intrinsic layer, indicating a greater recombination rate in the thicker samples. Previously, we found that the dark J-V characteristics of a-Si:H solar cells are largely independent of the intrinsic layer thickness. This phenomenon could be explained with a weak dependence of thickness on the recombination width, which is smaller than the intrinsic layer thickness. However, in the nc-Si:H solar cells, the dark J-V characteristics, especially the J_0, strongly depend on the intrinsic layer thickness. A thicker intrinsic layer results in a larger J_0, which could indicate that the recombination width is the same as the intrinsic layer thickness. A time-of-flight measurement found that the hole mobility in nc-Si:H is over one hundred times larger than in a-Si:H [32]. Correspondingly, the hole diffusion length in nc-Si:H solar cells is much larger than in a-Si:H solar cells and the improved hole diffusion length leads to a recombination width similar to the intrinsic layer thickness.

We now discuss the main points obtained from the experimental results. First, we know that the FF usually decreases with an increase in the intrinsic layer thickness because of the reduction of built-in electric field and increased recombination rate. The intrinsic layer thickness dependence of FF in the nine samples follows this common trend. It is also understandable that the J_{sc} increases with increased intrinsic layer thickness since the light absorption is increased. Here, we need to point out that this is true for the cells with a certain thickness range. Beyond

Table XV. The dark J-V fitting results of three nc-Si:H cells with different intrinsic layer thicknesses. The *i/p* buffer layer is the same for the samples (7 minutes). J_0 denotes the reverse saturated current, and n the diode quality factor.

Sample No.	*i* layer deposition time	J_0 (A/cm^2)	n
14113	7 min	3×10^{-8}	1.75
14114	15 min	6×10^{-8}	1.67
14106	30 min	2×10^{-7}	1.70

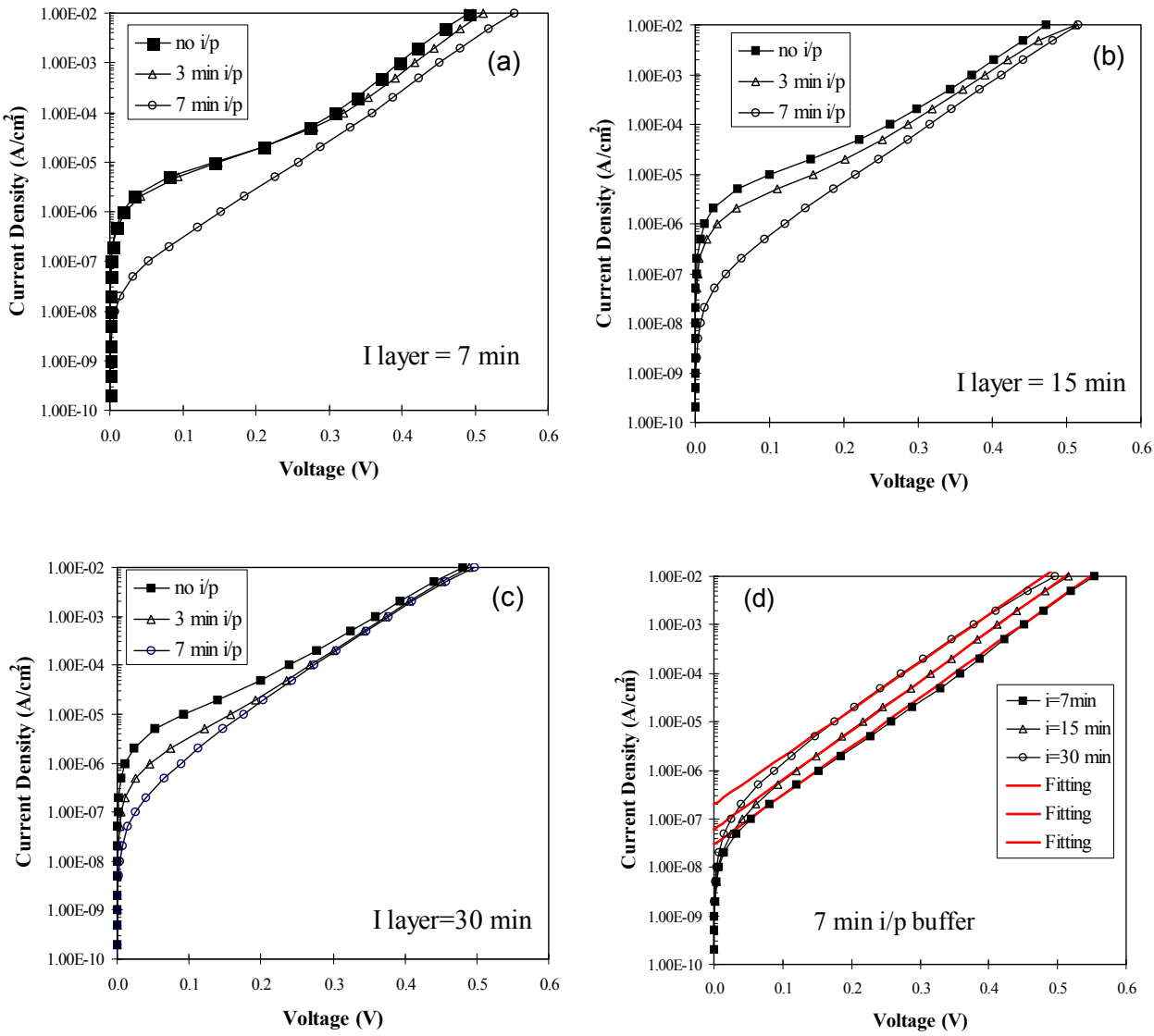

Figure 11. Dark *J-V* characteristics of the cells with (a) a 7-minute intrinsic layer but with different *i/p* buffer thicknesses; (b) a 15-minute intrinsic layer but with different *i/p* buffer layer thicknesses; (c) 30-minute intrinsic layer but with different *i/p* buffers; (d) different intrinsic layer thicknesses but with the same *i/p* buffer layer thickness of 7 minutes.

this range, other factors such as microstructure evolution, carrier collection length, or collapse of the built-in electric field, might play dominant roles. Compared to the FF and J_{sc}, the effect of intrinsic layer thickness on the V_{oc} is more complicated. Previously, we found that the V_{oc} decreases with increasing thickness more dramatically in nc-Si:H than in a-Si:H solar cells [8]. One explanation was the evolution of crystalline volume fraction with the intrinsic layer thickness. A similar trend is also observed in these nine samples as listed in Table XII. The reason for a small V_{oc} change with the intrinsic layer thickness for the cells with no or thin *i/p* buffer is probably due to the large shunt current density or a large recombination current density in the *i/p* interface. This is consistent with the results from the dark J-V measurements. With the increase of the *i/p* buffer layer thickness to 7 minutes, the shunt-current or interface recombination current was reduced, and the V_{oc} monotonically decreased with the intrinsic layer thickness. Moreover, from the Raman measurements, we noticed that the increase of crystalline volume fraction with the intrinsic layer thickness is small, which could not be the dominant factor for the reduced V_{oc} in the thicker cells made with hydrogen dilution profiling. Instead, the significantly increased dark current density could be the main reason for the reduced V_{oc} in the thicker cells. Second, we found that the V_{oc} increases with an increase in the *i/p* buffer layer thickness. This is because the a-Si:H *i/p* buffer layer reduces the shunt current density. This was confirmed by the dark J-V measurements as shown in Figure 11 (a), (b), and (c). We know that in the light J-V measurement, the V_{oc} is obtained when the dark current equals photo current. The larger the dark current is, the smaller the V_{oc}. We also found that the FF is not improved for these cells when the buffer layer was added. This is probably because the a-Si:H *i/p* buffer is too thick and introduces an extra series resistance. Another interesting observation is that the *i/p* buffer has a larger effect on the thin cells than thick ones. It may indicate that the cell performance of the thin samples was dominated by the *i/p* interface, while the performance of the thick samples was dominated by the bulk properties.

A stability study has been carried out on the nine nc-Si:H solar cells, and the results are listed in Table XVI. As a comparison, four high rate a-Si:H solar cells with different intrinsic layer thicknesses were also studied, and the results are listed in Table XVII. Three points have been observed from the tables. First, the light-induced degradation rate in nc-Si:H decreases with increasing intrinsic layer thickness. This is different from the case in a-Si:H based solar cells, where we usually found that the degradation rate increases with the intrinsic layer thickness. Second, adding an *i/p* buffer layer reduces the degradation rate, especially for the thin solar cells. For example, sample 14098 with no *i/p* buffer degrades ~14% in efficiency, whereas sample 14113 with a 7-minute *i/p* buffer layer degrades only ~ 2%. However, for the thick samples, the degradation rate does not change much when the *i/p* buffer layer is changed, which can be seen by comparing sample 14100 with no *i/p* buffer and sample 14106 with a 7-minute *i/p* buffer layer. To clearly see this trend, we plotted the degradation rate versus the intrinsic layer thickness in Fig. 12. Third, the degradation (if any) happens mostly in V_{oc} and FF. J_{sc} shows almost no degradation for all the samples.

As discussed above, the cell performance in thin cells is mainly dominated by the *i/p* interface. Since light soaking causes more damage in the *i/p* interface than in the bulk due to more exposure, the thin cells will be subjected to more degradation than the thick cells. Moreover, according to our experience, the V_{oc} and FF are more sensitive to the *i/p* interface than J_{sc}. Any change in the *i/p* interface will affect the V_{oc} and FF. This is in agreement with the observation in the third point. Improving the interface by adding high quality amorphous *i/p* buffer should also reduce the light-induced degradation in the *i/p* interface region. This explains

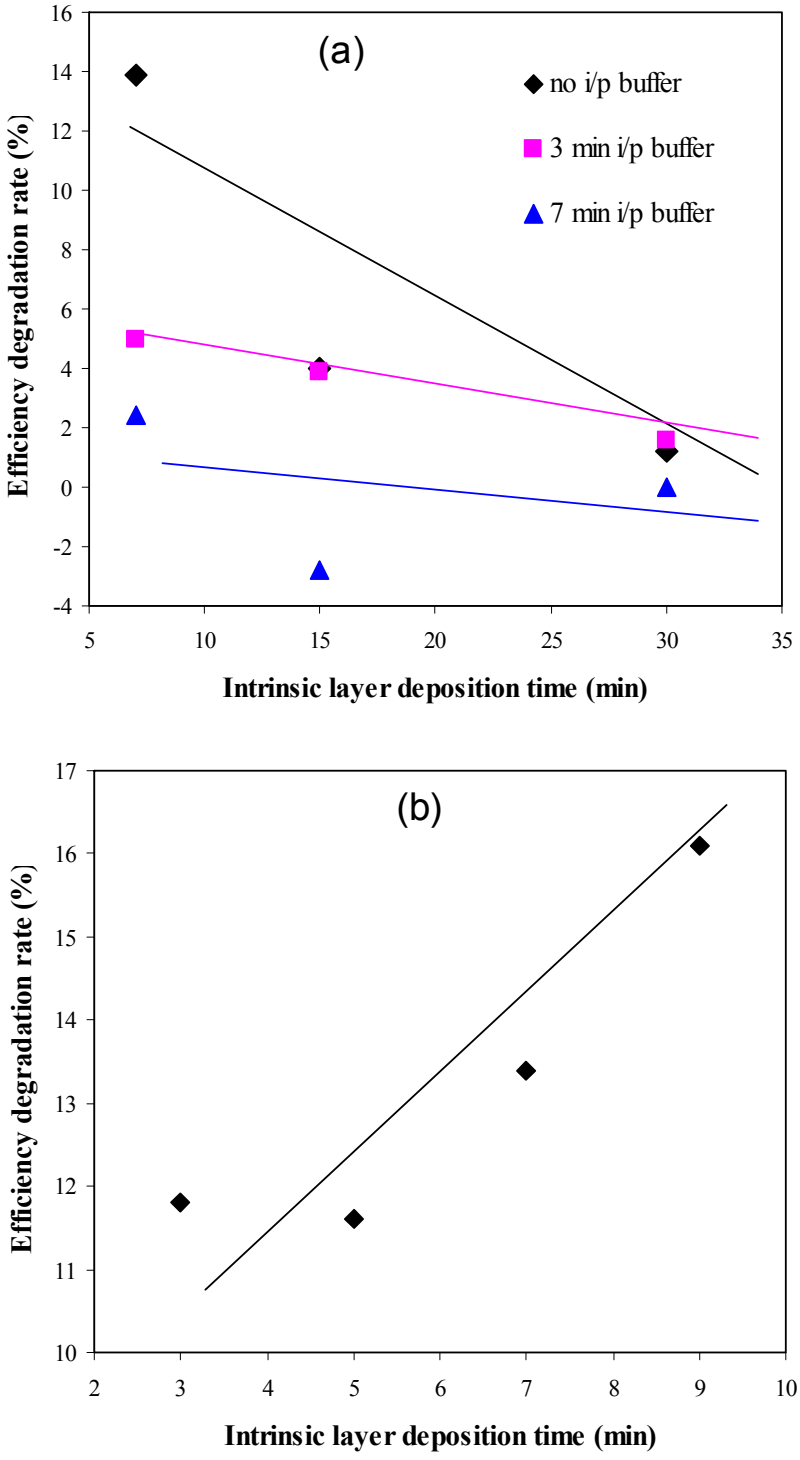

Figure 12. (a) Efficiency degradation rate as a function of intrinsic layer deposition time in nc-Si:H solar cells. The thicknesses are in the range of 350 to 900 nm; (b) Efficiency degradation rate as a function of intrinsic layer deposition time in a-Si:H solar cells. The thicknesses are in the range of 100 to 300 nm.

Table XVI. Stability results of nc-Si:H solar cells with different intrinsic and *i/p* buffer layer thicknesses.

Sample No.	Time (i) (min)	Time(i/p) (min)	Status	V_{oc} (V)	FF	Q (mA/cm^2)	P_{max} (mW/cm^2)
14098	7	0	Initial	0.463	0.714	14.54	4.81
			Stable	0.422	0.672	14.60	4.14
			Deg.(%)	-8.9%	-5.9%	0	-13.9%
14099	15	0	Initial	0.455	0.641	18.71	5.46
			Stable	0.433	0.641	18.90	5.25
			Deg.(%)	-4.8%	0	+1.0%	-4.0%
14100	30	0	Initial	0.455	0.586	22.49	6.00
			Stable	0.443	0.586	22.83	5.93
			Deg.(%)	-2.6%	0	+1.5%	-1.2%
14101	7	3	Initial	0.481	0.700	14.18	4.77
			Stable	0.462	0.673	14.57	4.53
			Deg.(%)	-4.0%	-3.9%	+2.8%	-5.0%
14111	15	3	Initial	0.473	0.642	18.78	5.70
			Stable	0.448	0.646	18.92	5.48
			Deg.(%)	-5.3%	+0.6%	+0.7%	-3.9%
14112	30	3	Initial	0.473	0.590	22.87	6.38
			Stable	0.459	0.597	22.91	6.28
			Deg.(%)	-3.0%	+1.2%	+0.2%	-1.6%
14113	7	7	Initial	0.532	0.677	16.00	5.76
			Stable	0.516	0.679	16.04	5.62
			Deg.(%)	-3.0%	0	0	-2.4%
14114	15	7	Initial	0.491	0.622	19.73	6.03
			Stable	0.492	0.646	19.51	6.20
			Deg.(%)	0	+3.9%	-1.1%	+2.8%
14106	30	7	Initial	0.483	0.590	22.82	6.50
			Stable	0.481	0.597	22.62	6.50
			Deg.(%)	0	+1.2%	-0.9%	0

Table XVII. Stability results of high rate a-Si:H solar cells with different intrinsic layer thicknesses. The cells were deposited using MVHF on Ag/ZnO coated stainless steel substrates.

Sample No.	Status	Q (mA/cm^2)	V_{oc} (V)	FF	P_{max} (mW/cm^2)	Thickness (nm)
14672	Initial	9.12	1.021	0.755	7.03	104
	Stable	8.93	0.977	0.711	6.20	
	Deg.	2.1%	4.3%	5.8%	11.8%	
14671	Initial	11.11	0.987	0.744	8.16	156
	Stable	10.77	0.970	0.690	7.21	
	Deg.	3.1%	1.7%	7.3%	11.6%	
14673	Initial	12.87	0.999	0.716	9.21	235
	Stable	12.32	0.973	0.666	7.98	
	Deg.	4.3%	2.6%	7.0%	13.4%	
14674	Initial	13.77	1.001	0.690	9.51	307
	Stable	12.97	0.973	0.632	7.98	
	Deg.	5.8%	2.8%	8.4%	16.1%	

the reduced light-induced degradation rate by adding an *i/p* buffer layer. Previously, it has been reported that the bulk properties are improved by using a hydrogen dilution profiling technique [15], but actually the main improvement occurs close to the *i/p* interface region due to decreased hydrogen dilution. Based on the same argument, it is not surprising that the thick cells with an optimized *i/p* buffer have stable performance.

The dark J-V characteristics of the nine nc-Si:H solar cells after light soaking are plotted in Fig. 13. Compared to the corresponding initial results, all dark J-V curves are shifted upward, indicating an enhanced recombination rate after light soaking. It is noticed that a larger V_{oc} decrease corresponds to a larger dark current increase. For the cells with a thicker *i/p* buffer (7-minute *i/p* buffer), the curves are shifted in parallel. However, for the cells with no *i/p* buffer, the shunt current (low voltage part) does not change. Only the recombination current (high voltage part) increased after light soaking.

In summary, the effects of the intrinsic and *i/p* buffer layer thicknesses on nc-Si:H cell performance and stability have been studied. The results show that the *i/p* buffer layer not only has a large effect on cell performance, but also on the stability. For the cells with a thin intrinsic layer, the cell performance, especially V_{oc}, is limited by the *i/p* interface. An optimized *i/p* buffer layer can improve the cell performance significantly. For the thick cells, the cell performance is limited by the bulk properties of the intrinsic layer. In this case, the buffer layer effect becomes less obvious. We also found that the stability dependence on intrinsic layer thickness for nc-Si:H cells is different from a-Si:H cells. The results were explained in terms of different contributions from the bulk properties of the intrinsic layer and the *i/p* interface layer.

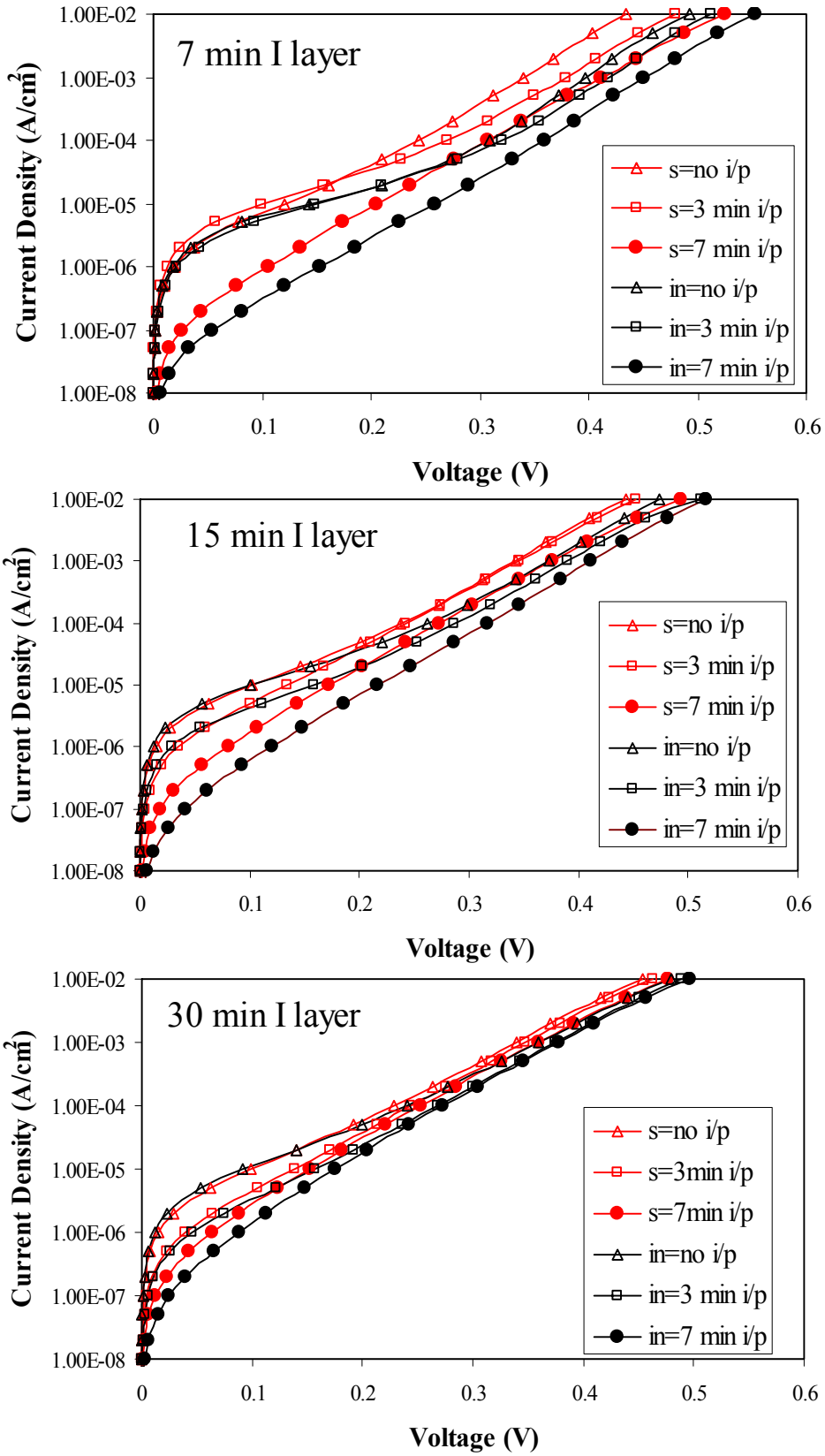

Figure 13. Dark *J-V* characteristics of nine nc-Si:H cells before and after light-soaking. Initial state is denoted by "in", and stabilized state is denoted by "s".

3.4. High Efficiency Hydrogenated Amorphous Silicon Based Triple-Junction Solar Cells Incorporating Nanocrystalline Silicon

We have used the knowledge gathered in the device design optimization, deposition process optimization, and material characterization to improve our nc-Si:H single-junction and multi-junction solar cells. We have made significant progress in improving the cell performance. We have achieved an initial active-area efficiency of 15.1% using an a-Si:H/a-SiGe:H/nc-Si:H triple-junction structure and 14.1% using an a-Si:H/nc-Si:H/nc-Si:H triple-junction structure The major contribution to the high efficiency triple-junction cell is the improved nc-Si:H bottom cell. Two important techniques were used for the optimization of the nc-Si:H material quality. First, a proper hydrogen dilution profiling was used to control the evolution of nanocrystallites along the growth direction. We found that the hydrogen dilution profiling improves not only the nc-Si:H cell performance [15], but also the stability [10]. Second, the nc-Si:H intrinsic layer was deposited in a high pressure and high power regime [4,33]. Under this condition, the quality of the high rate deposited nc-Si:H material is improved. Table XVIII lists the J-V characteristics of nc-Si:H single-junction solar cells suitable for use in the middle and the bottom cells. An initial active-area cell efficiency of 8.99% has been achieved. Figure 14 shows the J-V characteristics and QE of the best nc-Si:H single-junction cell. This cell shows a large V_{oc} but a moderate J_{sc}, which is suitable for the middle cell in triple-junction structures. We light soaked the high efficiency nc-Si:H cell under 100 mW/cm^2 white light at 50 °C for over 1000 hours and obtained a stabilized efficiency of 8.5%. The 5.5% light-induced degradation is mainly due to a reduction in the J_{sc}. The QE curve reveals a reduction in the short wavelength region, which does not affect its performance in a multi-junction structure. We have also developed nc-Si:H single-junction cells with high long wavelength response for the bottom cell in triple-junction structures. Figure 15 shows the J-V characteristics and QE of the best nc-Si:H cell used as the bottom cell in a triple-junction structure. The total current density is ~27 mA/cm^2 with long wavelength response extending to 1100 nm.

We used the optimized component cells to fabricate triple-junction cells. Table XIX lists the J-V characteristics of several a-Si:H/a-SiGe:H/nc-Si:H cells in the initial and light-soaked states, where the light-soaked state was reached by light soaking under ~100 mW/cm^2 white light at 50 ºC for 575 hours. The highest initial active-area efficiency of 15.1% is achieved using this triple-junction structure. The initial J-V characteristics and QE are shown in Fig. 16. After light soaking, a stable efficiency of 13.0% is obtained. From the data in Table XIX, one can see that

Table XVIII: Initial active-area performance of nc-Si:H solar cells made with MVHF at high rates.

Sample	Eff (%)	J_{sc} (mA/cm^2)	V_{oc} (V)	FF	Comment
13831	8.99	23.59	0.568	0.671	middle
13821	8.65	24.44	0.552	0.641	
13829	8.48	23.11	0.566	0.648	
13935	8.81	26.94	0.538	0.608	bottom
14173	7.78	26.65	0.500	0.584	
14191	7.86	26.36	0.478	0.624	

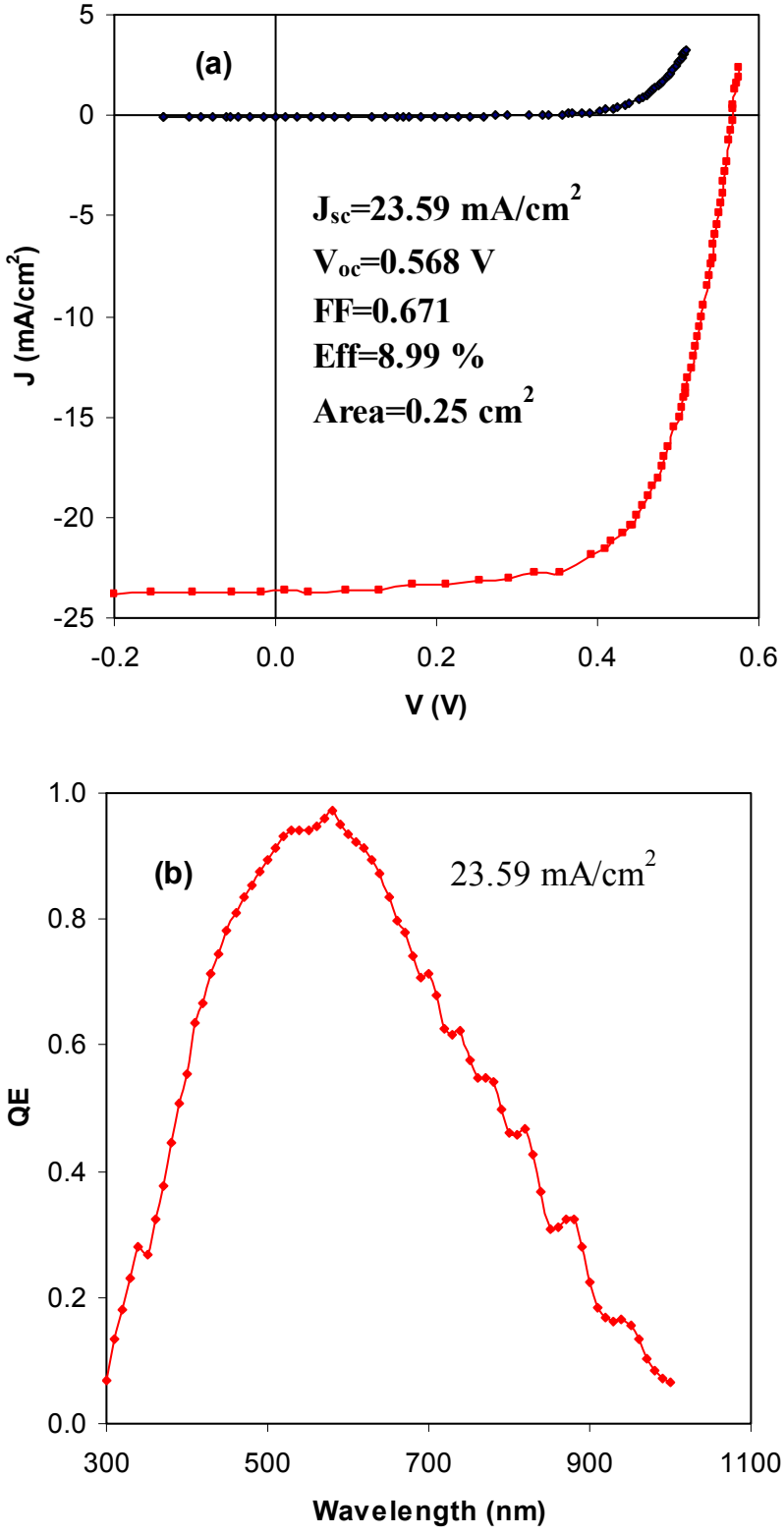

Figure 14. (a) J-V characteristics and (b) quantum efficiency of a nc-Si:H solar cell as the middle cell in a triple-junction structure.

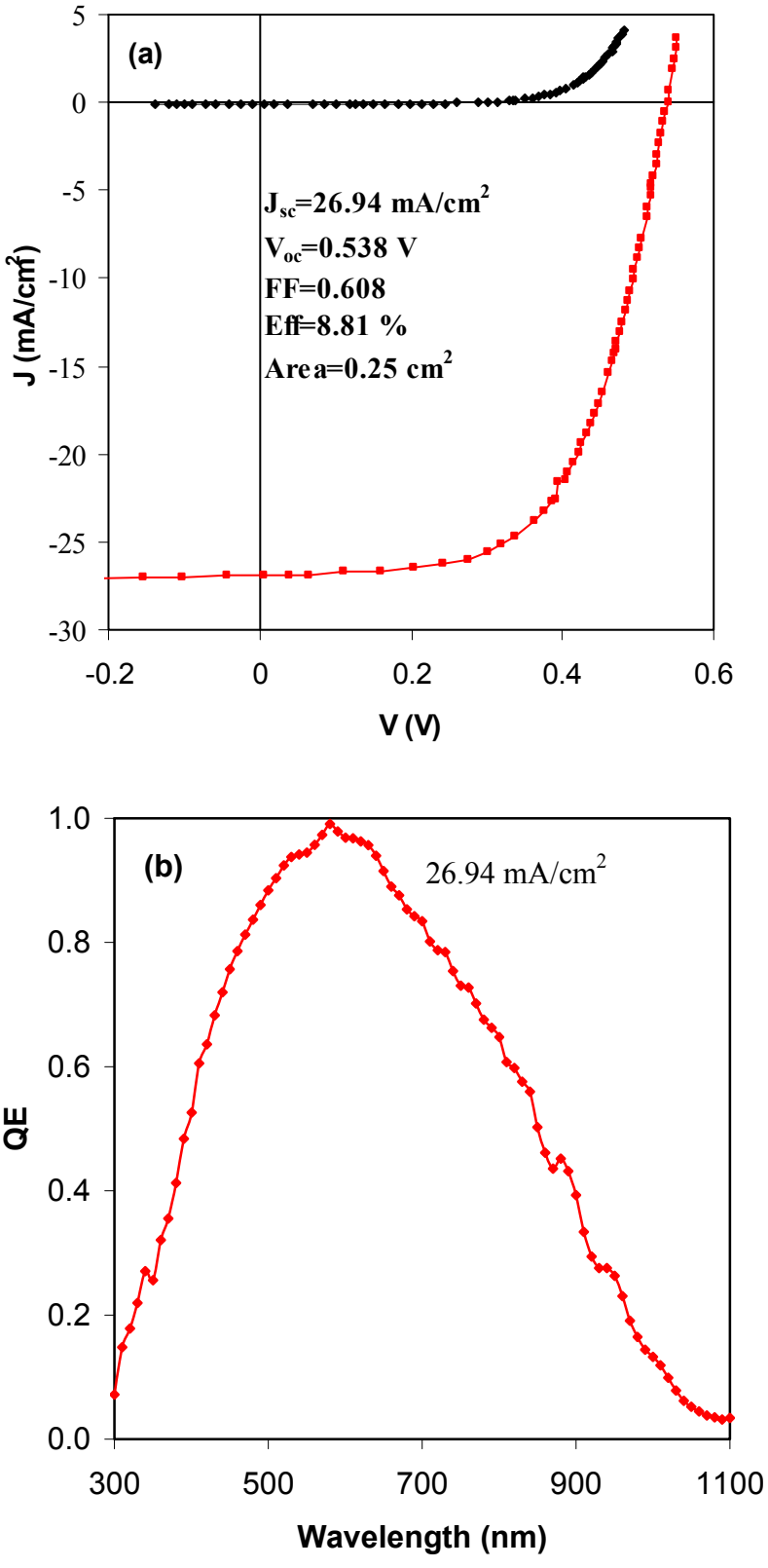

Figure 15. (a) J-V characteristics and (b) quantum efficiency of a nc-Si:H solar cell as the bottom cell in a triple-junction structure.

Table XIX. J-V characteristics of high efficiency a-Si:H/a-SiGe:H/nc-Si:H triple-junction solar cells. Deg. denotes the percentage of light-induced degradation. The bold numbers are the highest efficiencies and italic numbers are the limited current densities for J_{sc}.

Sample	State	Eff (%)	J_{sc} (mA/cm^2)	QE (mA/cm^2)			V_{oc} (V)	FF
				top	middle	bottom		
15501-34	Initial	14.77	9.11	*9.11*	9.24	9.20	2.145	0.756
	Stable	12.62	8.69	8.85	*8.69*	9.12	2.101	0.691
	Deg.	14.6%	4.6%	2.9%	6.0%	0.9%	2.1%	8.6%
15506-33	Initial	**15.07**	9.13	*9.13*	9.27	9.31	2.195	0.752
	Stable	12.49	8.63	8.74	*8.63*	9.24	2.116	0.684
	Deg.	17.1%	5.5%	4.3%	6.9%	0.8%	3.6%	9.0%
15506-34	Initial	14.27	8.74	9.25	9.41	*8.74*	2.167	0.755
	Stable	**12.98**	8.74	8.97	8.88	*8.74*	2.110	0.704
	Deg.	9.0%	0	3.0%	5.6%	0	2.6%	6.7%

the bottom cell current did not degrade after light soaking; having the bottom cell limited current mismatching resulted in the lowest degradation. The light-induced degradation is only 9.0%. However, the cell with the highest initial efficiency degraded by 17.1%, mainly due to a large reduction of FF caused by the middle cell limited current mismatching.

Table XX summarizes the J-V characteristics of several a-Si:H/nc-Si:H/nc-Si:H triple-junction solar cells in the initial and light-soaked states, where the light-soaked state was reached by light soaking under ~100 mW/cm^2 white light at 50 ºC for over 1000 hours. The highest initial active-area efficiency of 14.1% is achieved with the initial J-V characteristics and QE shown in Fig. 17. Although the a-Si:H/nc-Si:H/nc-Si:H triple-junction structure does not yield the highest initial efficiency, it shows a very small light-induced degradation of 4.3%, resulting from a better stability of the nc-Si:H middle cell compared to the a-SiGe:H middle cell. A stable active-area efficiency of 13.3% is also achieved with this cell structure.

Table XX. J-V characteristics of high efficiency a-Si:H/nc-Si:H/nc-Si:H triple-junction solar cells. Deg. denotes the percentage of light-induced degradation. The bold numbers are the highest efficiencies and italic numbers are the limited current densities for J_{sc}.

Sample	State	Eff (%)	J_{sc} (mA/cm^2)	QE (mA/cm^2)			V_{oc} (V)	FF
				top	middle	bottom		
13955-33	Initial	**14.14**	9.11	9.11	9.72	*9.11*	1.965	0.790
	Stable	13.19	8.79	*8.79*	9.56	9.04	1.947	0.771
	Deg.	6.7%	3.5%	3.5%	1.6%	0.8%	0.9%	2.4%
13955-24	Initial	13.86	8.89	9.02	9.52	*8.89*	1.981	0.787
	Stable	**13.26**	8.72	8.75	9.25	*8.72*	1.973	0.771
	Deg.	4.3%	1.9%	3.0%	2.8%	1.9%	0.4%	2.0%
14005-33	Initial	13.67	8.99	9.44	9.54	*8.99*	1.944	0.782
	Stable	13.24	8.92	9.04	9.42	*8.92*	1.933	0.768
	Deg.	3.1%	0.8%	4.2%	1.3%	0.8%	0.6%	1.8%

In summary, we have made significant progress in the optimization of a-Si:H, a-SiGe:H, and nc-Si:H materials and devices for high efficiency triple-junction solar cells. The a-Si:H top and a-SiGe:H middle cells have been re-optimized for matching the high current from the nc-Si:H bottom cell. The nc-Si:H bottom cell has been improved using MVHF in the high pressure regime. An optimized hydrogen dilution profiling is the key technique for optimizing the growth of the nc-Si:H material, which is a critical element for obtaining high efficiency nc-Si:H solar cells. Based on these techniques, we have achieved initial and stable active-area efficiencies of 15.1% and 13.0%, respectively, using the a-Si:H/a-SiGe:H/nc-Si:H triple-junction structure. The stability of triple-junction cells is improved by substituting the a-SiGe:H middle cell by nc-Si:H. Using the a-Si:H/nc-Si:H/nc-Si:H triple-junction structure, we have obtained an initial active-area efficiency of 14.1%. After prolonged light soaking, the a-Si:H/nc-Si:H/nc-Si:H triple-junction cell stabilized at 13.3%. The stable triple-junction cell efficiency incorporating nc-Si:H material is higher than the previous record of 13.0% achieved using the conventional a-Si:H/a-SiGe:H/a-SiGe:H triple-junction structure.

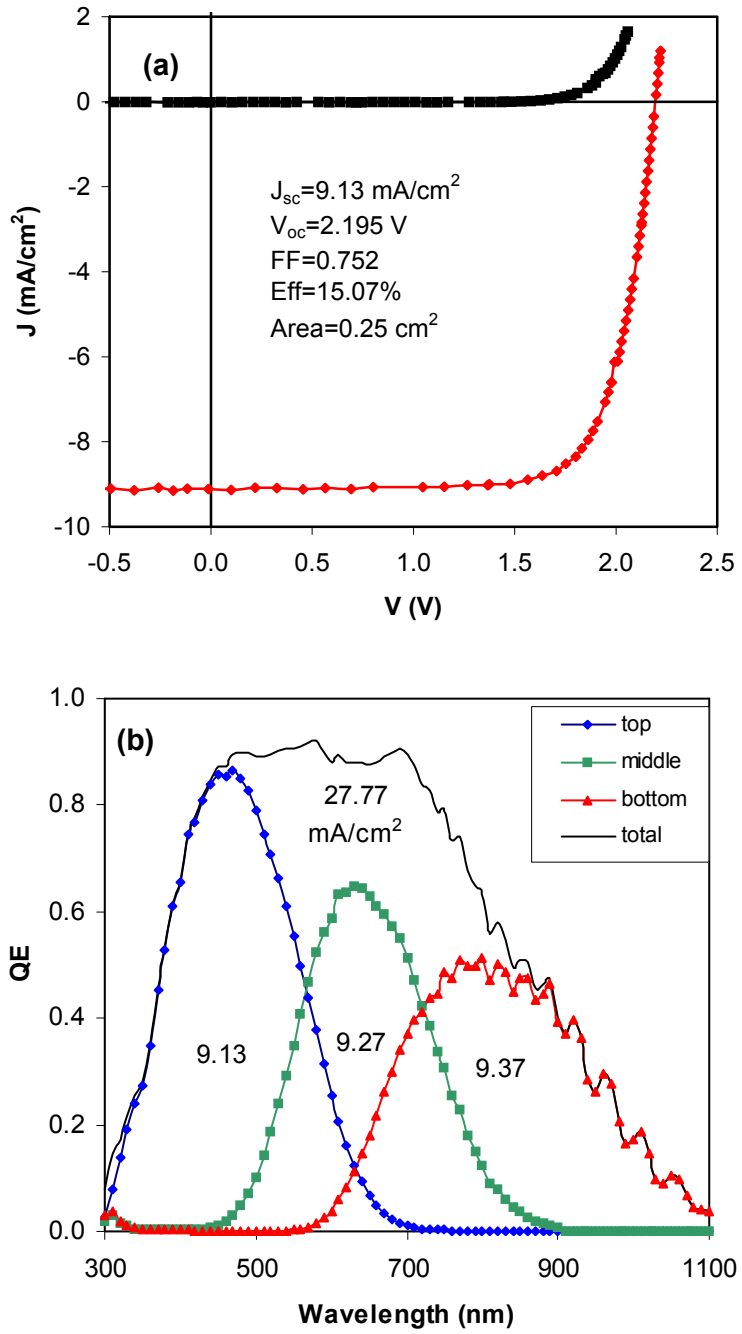

Figure 16. (a) J-V characteristics and (b) quantum efficiency of an a-Si:H/a-SiGe:H/nc-Si:H triple-junction solar cell.

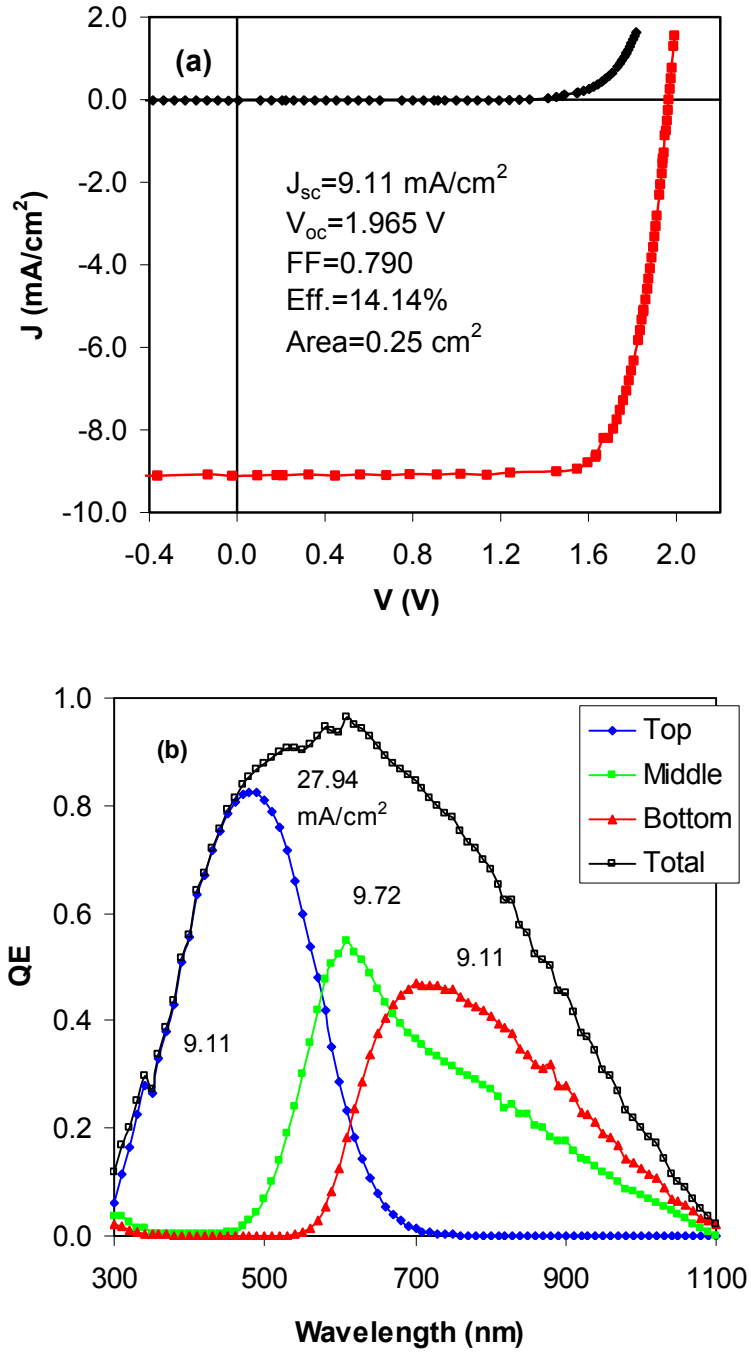

Figure 17. (a) J-V characteristics and (b) quantum efficiency of an a-Si:H/nc-Si:H/nc-Si:H triple-junction solar cell.

REFERENCES

[1] K. A. Emery, C. R. Osterwald, T. W. Cannon, D. R. Myers, J. Burdick, T. Glatfelter, W. Czubatyj, and J. Yang, Proceeding of 18th IEEE Photovoltaic Specialist Conference, (IEEE, 1985), p. 623.

[2] A. Shah, J. Dutta, N. Wyrsch, K. Prasad, H. Curtins, F. Finger, A. Howling, and Ch. Hollenstein, Mater. Res. Soc. Symp Proc. **258**, 15 (1992).

[3] J. Meier, P. Torres, R. Platz, S. Dubail, U. Kroll, J. A. Anna Selvan, N. Pellaton Vaucher, Ch. Hof, D. Fischer, H. Keppner, A. Shah, K.-D. Ufert, P. Giannoulès, J. Koehler, Mater. Res. Soc. Symp. Proc. **420**, 3 (1990).

[4] Y. Mai, S. Klein, R. Carius, J. Wolff, A. Lambertz, F. Finger, and X. Geng, J. Appl. Phys. **97**, 114913 (2005).

[5] T. Matsui, A. Matsuda, and M. Kondo, Mater. Res. Soc. Symp Proc. **808**, 557 (2004).

[6] J. Yang, S. Sugiyama, and S. Guha, Mater. Res. Soc. Symp Proc. **507**, 157 (1998).

[7] J. Yang, B. Yang, J. Smeets, and S. Guha, Mater. Res. Soc. Symp Proc. **664**, A11.3 (2001).

[8] B. Yan, G. Yue, J. Yang, A. Banerjee, and S. Guha, Mater. Res. Soc. Symp. Proc. **762,** 309 (2003).

[9] B. Yan, G. Yue, J. Yang, K. Lord, A. Banerjee, and S. Guha, Proc. of 3rd World Conference on Photovoltaic Energy Conversion*,* May 11-18, 2003, Osaka, Japan, p. 2773.

[10] G. Yue, B. Yan, G. Ganguly, J. Yang, S. Guha, C. W. Teplin, and D.L. Williamson, Proc. of 4th World Conference on Photovoltaic Energy Conversion, May 7-12, 2006, Hawaii, USA, p. 1588.

[11] J. Yang, A. Banerjee, and S. Guha, Appl. Phys. Lett. **70**, 2975 (1997).

[12] S. Guha, Mater. Res. Soc. Symp. Proc. **808***,* 521 (2004).

[13] K. Yamamoto, *et al*., Technical Digest, 15th International Photovoltaic Science and Engineering Conference, Shanghai, China, October 10-15, 2005, p. 529.

[14] K. Saito, M. Sano, S. Okabe, S. Sugiyama, and K. Ogawa, Sol. Energy Mater. & Solar Cells **86**, 565 (2005).

[15] B. Yan, G. Yue, J. Yang, S. Guha, D. L. Williamson, D. Han, and C.-S. Jiang, Appl. Phys. Lett. **85**, 1955 (2004).

[16] B. Yan, J. M. Owens, J. Yang, and S. Guha, Proc. of 31st IEEE Photovoltaic Specialists Conference, Lake Buena Vista, FL, January 3-7, 2005, p. 1456.

[17] J. Meier, R. Flückiger, H. Keppner, and A. Shah, Appl. Phys. Lett. **65**, 860 (1994).

[18] O. Vetterl, F. Finger, R. Carius, P. Hapke, L. Houben, O. Kluth, A. Lambertz, A. Mück, B. Rech, and H. Wagner, Sol. Energy Mater. Sol. Cells **62**, 97 (2000).

[19] K. Yamamoto, IEEE Trans. on Electron Device **46**, 2041 (1999).

[20] B. Yan, G. Yue, J. M. Owens, J. Yang, and S. Guha, Appl. Phys. Lett. **85**, 1925 (2004).

[21] G. Yue, B. Yan, J. Yang, and S. Guha, Appl. Phys. Lett. **86**, 092103 (2005).

[22] G. Yue, B. Yan, J. Yang, and S. Guha, J. Appl. Phys. **98**, 074902 (2005).

[23] S. Klein, F. Finger, R. Carius, T. Dylla, B. Rech, M. Grimm, L. Houben, and M. Stutzmann, Thin Solid Films **430**, 202 (2003).

[24] F. Meillaud, E. Vallat-Sauvain, X. Niquille, M. Dubey, J. Bailat, A. Shah, and C. Ballif, Proceeding of the 31st IEEE Photovoltaic Specialists Conference, Florida, USA, January 3-7, 2005, p. 1412.

[25] T. Roschek, T. Repmann, J. Müller, B. Rech, H. Wagner, Proceeding of 28th IEEE Photovoltaic Specialists Conference, Anchorage, AK, September 15-22, 2000, p. 150.
[26] S. Veprek, F.-A. Sarott, and Z. Iqbal, Phys. Rev. B **36**, 3344 (1987).
[27] E. Bustarret, M. A. Hachicha, and M. Brunel, Appl. Phys. Lett. **52**, 1675 (1988).
[28] D. Han, J. D. Lorentzen, J. Wenberg-Wolf, L. McNeil, and Q. Wang, J. Appl. Phys. **94**, 2930 (2003).
[29] D. V. Tsu, B. S. Chao, S. R. Ovshinsky, S. Guha, and J. Yang, Appl. Phys. Lett. **71**, 1317 (1997).
[30] D. V. Tsu, B. S. Chao, S. R. Ovshinsky, S. J. Jones, J. Yang, S. Guha, and R. Tsu, Phys. Rev. B **63**, 125338 (2001).
[31] A. Pawlikiewicz and S. Guha, Mat. Res. Soc. Symp. Proc. **118**, 599 (1988).
[32] T. Dylla, F. Finger, and E. A. Schiff, App. Phys. Lett. **87**, 032103 (2005).
[33] L. Guo, M. Kondo, M. Fukawa, K. Saitoh, and A. Matsuda, Jpn. App. Phys. Part 2 **37,** L1116 (1998).

REPORT DOCUMENTATION PAGE

Form Approved
OMB No. 0704-0188

PLEASE DO NOT RETURN YOUR FORM TO THE ABOVE ORGANIZATION.

1. REPORT DATE *(DD-MM-YYYY)*	2. REPORT TYPE	3. DATES COVERED *(From - To)*
July 2007	Subcontract Report	30 January 2006–29 January 2007

4. TITLE AND SUBTITLE
High-Efficiency Amorphous Silicon and Nanocrystalline Silicon-Based Solar Cells and Modules: Annual Technical Progress Report, 30 January 2006 – 29 January 29, 2007

5a. CONTRACT NUMBER
DE-AC36-99-GO10337

5b. GRANT NUMBER

5c. PROGRAM ELEMENT NUMBER

6. AUTHOR(S)
S. Guha and J. Yang

5d. PROJECT NUMBER
NREL/SR-520-41866

5e. TASK NUMBER
PVB75101

5f. WORK UNIT NUMBER

7. PERFORMING ORGANIZATION NAME(S) AND ADDRESS(ES)
United Solar Ovonic LLC
Troy, Michigan

8. PERFORMING ORGANIZATION REPORT NUMBER
ZXL-6-44205-14

9. SPONSORING/MONITORING AGENCY NAME(S) AND ADDRESS(ES)
National Renewable Energy Laboratory
1617 Cole Blvd.
Golden, CO 80401-3393

10. SPONSOR/MONITOR'S ACRONYM(S)
NREL

11. SPONSORING/MONITORING AGENCY REPORT NUMBER
NREL/SR-520-41866

12. DISTRIBUTION AVAILABILITY STATEMENT
National Technical Information Service
U.S. Department of Commerce
5285 Port Royal Road
Springfield, VA 22161

13. SUPPLEMENTARY NOTES
NREL Technical Monitor: Bolko von Roedern

14. ABSTRACT *(Maximum 200 Words)*

United Solar Ovonic LLC (United Solar) has successfully used its spectrum-splitting a-Si:H/a-SiGe:H/a-SiGe:H triple-junction structure in the two ~30 MW manufacturing plants, and will use the same technology in its next 60 MW plant in Greenville Michigan, which will start production in 2007. To improve the solar panel efficiency and reduce the manufacturing cost further, we have identified three areas of research for this project: i) Optimize the a-Si:H and a-SiGe:H deposition parameters under the current manufacturing constraints for improving the solar module efficiency and manufacturing throughput, and reducing the manufacturing cost; ii) Explore new deposition methods for a-Si:H and a-SiGe:H materials to improve the a-Si:H/a-SiGe:H/a-SiGe:H triple-junction cell efficiency at high deposition rate; and iii) Explore new materials and new cell structures for higher efficiency at high deposition rate.

15. SUBJECT TERMS
PV; amorphous silicon; nanocrystalline; solar cell; modules; triple-junction; manufacturer; optimization; throughput, high deposition rate; efficiency; cost;

16. SECURITY CLASSIFICATION OF:			17. LIMITATION OF ABSTRACT	18. NUMBER OF PAGES	19a. NAME OF RESPONSIBLE PERSON
a. REPORT	b. ABSTRACT	c. THIS PAGE			19b. TELEPHONE NUMBER (*Include area code)*
Unclassified	Unclassified	Unclassified	UL		

Standard Form 298 (Rev. 8/98)
Prescribed by ANSI Std. Z39.18